UNITED STATES ATOMIC ENERGY COMMISSION
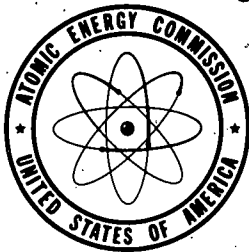
UCRL-2424

CROSS SECTIONS FOR PRODUCTION OF π^+-MESONS BY 335-MEV PROTONS AS A FUNCTION OF ATOMIC NUMBER (thesis)

By
Jack Merritt

November 1953

Radiation Laboratory
University of California, Berkeley

DISCLAIMER

DISCLAIMER

Portions of this document may be illegible in electronic image products. Images are produced from the best available original document.

ABSTRACT

The relative yield of π^+-mesons has been determined for 335-Mev protons on a number of elements. Specifically, the relative differential cross-section, $d^2\sigma/dEd\Omega$, was measured at $0° \pm 4°$ in the reaction

$$p + A \rightarrow \pi^+ + A'$$
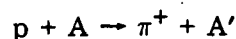
for the elements D, Be^9, B^{10}, B(natural), C, Al, Cu, Fe, Ag, and Pb. The π^+-meson energies ranged from 35 to 145 Mev. They were counted electronically from signals generated in a trans-stilbene crystal telescope. Identification of the π^+-meson depended upon a fast coincidence in the first two crystals plus the $\pi - \mu$ decay in the third crystal of the telescope.

No special isotope effects were observed for the Be^9, B^{10}, B(natural) and C spectra.

For C, Al, Fe, Ag and Pb the relative yield per nucleus can be explained by proton and meson attenuation within the nucleus. The attenuation of protons and mesons is consistent with mean free paths which have been measured in other experiments for protons and mesons in nuclear matter.

CROSS SECTIONS FOR PRODUCTION OF π^+-MESONS BY 335-MEV PROTONS AS A FUNCTION OF ATOMIC NUMBER

Jack Merritt

Radiation Laboratory, Department of Physics,
University of California, Berkeley, California

November, 1953

I INTRODUCTION

The production of mesons by high-energy protons on nuclei has been investigated actively in the last few years. Of the many questions concerning the production of mesons, the following two were selected for study:

1. How does the π^+-meson spectrum depend upon the type of nucleus?

2. What interpretation can be given to the observed meson spectrum?

Some partial answers to the first question are given. As for interpretation, an extremely crude nuclear model suffices to give the meson-yield dependence on the atomic number of the struck nucleus. More refined nuclear models could have been used, but such refinements seem unjustified in the present state of meson theory. A more satisfying interpretation of the data will probably have to wait for a clearer understanding of the elementary pion-nucleon interaction. Nevertheless the fact that a crude model, compatible with the data, can be made gives one confidence that he is on the right track. In the meantime the data will be of use in the design of other meson experiments and the calculation of corrections for such experiments.

The following sequence of cyclotron runs was made.

Series	Run	Target	Meson Kinetic Energy(Mev)
I	1	C, Al, Fe, Cu, Ag, Pb	53
II	2	Be^9, B^{10}, B(natural)C^{12}	34, 51, 69, 88, 110, 128
III	3	C, Cu, Pb	52 and 88
	4	C, Cu, Pb	147
IV	5	Deuterium Gas pressure 1,000 psi	complete spectrum between 50 and 150
	6	Deuterium Gas pressure 2,000 psi	complete spectrum between 50 and 150

A given run lasted two or three days.

Series I was a general survey.

Series II was to ascertain if there were any special isotope effects. From the first two series it appeared that the individual spectra would not vary radically between neighboring nuclei.

In series III the elements and meson energies to be measured were cut to a minimum in order to get better statistics on individual points.

The π^+-meson spectrum was measured for deuterium in series IV. The deuterium nucleus is sufficiently simple so that a detailed analysis may be possible.

Prior to and during the execution of the above work a good many experiments were done elsewhere to determine the dependence of π^+-, π^--, and π^0-meson production on the type nuclear species. Both protons and x-rays were used for exciting the nucleus. Before these experiments are discussed, some of the concepts useful in the explanation of pion production by protons on complex nuclei are listed:

(a) At high energies, the production of mesons probably occurs by collision between the incident proton and one nucleon rather than several nucleons. A justification for this point of view is that the separation between nucleons, approximately 2.8×10^{-13} cm, is large compared to $\lambdabar = 0.2 \times 10^{-13}$ cm for the incident 335-Mev proton. $\lambdabar \equiv$ de Broglie wave length$/2\pi$. In addition the struck nucleon is to be thought of as free and having some appropriate momentum distribution.

(b) As the incident protons pass through the nucleus they are attenuated by competing processes: $\lambda_p \equiv$ proton mean free path for all other processes competing with meson production.

(c) The mesons are attenuated by reabsorption as they pass through nuclear matter. $\lambda_m \equiv$ mean free path for meson absorption.

(d) The exclusion principle forbids collisions that leave the final nucleons in filled energy states.

(e) The Coulomb barrier does not inhibit the escape of mesons that have a kinetic energy in the range above 50 Mev.

In the limiting case of strong attenuation within the nucleus of either the incident proton or the escaping meson, the meson production is proportional to nuclear area. In fact the first interpretations were based on these ideas.

The earliest work on meson yields as a function of atomic number was done by R. F. Mozley[1], who bombarded various elements with 317 Mev x-rays. He measured relative values for $d^2\sigma/dE\,d\Omega$ at $90° \pm 8°$ for the following elements: H, Li, Be, C, Al, Cu, Sn and Pb. Two meson energies, 42 ± 7 Mev and 76 ± 6 Mev, were observed. To analyse his data it is useful to define the relative yield per proton:

$$\text{Relative yield per proton} \equiv \frac{\text{Relative differential cross section per nucleus}}{\text{Atomic number of the nucleus}}$$

The relative yield per proton is a maximum for hydrogen and decreases monotonically with Z. The drop in cross section per proton in going from H to Li was explained by the exclusion principle. The phase space available to the residual neutron is less for Li than for H. Two alternate explanations were offered for the gradual drop from Li to Pb. The first assumed that only the surface nucleons participated in the production. The second explanation assumed that the mean free path for meson reabsorption had to be less than 7×10^{-13} cm.

R. M. Littauer and D. Walker[2] studied the production of mesons at $135°$ by 310 Mev x-ray bombardment of various nuclei. The meson energy was 65 ± 15 Mev. They observed a remarkable correlation between production cross section and binding energy of the struck nucleus. They also observed that the sum of the π^+ and π^- production cross sections varied as the geometrical area of the nucleus.

The first work to be reported on the production of mesons by proton bombardment of various nuclei was done by D. L. Clark[3a, b]. He observed relative values of $d^2\sigma/dE\,d\Omega$ for the production of 40-Mev π^+-mesons at 130° to 150° and π^--mesons at 30° to 50° by 240-Mev protons on Be, C, Al, Cu, Ag, W and Pb. Clark's cross sections vary roughly as the geometrical cross section of the struck nucleus, but with important deviations. He pointed out that the production cross section varied more nearly as the proton-absorption cross section; namely as A when A is small and as $A^{2/3}$ when A is large. When he plotted his differential cross section divided by $A^{2/3}$ he found a maximum for Al in the case of π^+ production and a general falling off at the beginning and end of the periodic table. R. E. Marshak pointed out that this effect may be correlated with the extra binding energy available in the struck nucleus.[4]

Though the statistics were poor, the data of series I run 1[5] were consistent with a production cross section proportional to the geometrical area of the struck nucleus.

M. M. Block, S. Passman and W. W. Havens[6] have bombarded C, Cu, and Pb with 381-Mev protons and observed the meson spectra coming off at 90°. R. Sagane and W. F. Dudziak[7a, b] measured the production of 12.5-, 27-, and 33-Mev π^+-mesons at 90° produced by 340-Mev proton bombardment of Be, C, Al, Cu, Ag and Pb.

A summary of the data for the experiments above is given in Fig. 9. The general trend of meson yield plotted against atomic mass A is similar for the different experiments.

It is suggested that the reader skip to the section Results and Interpretation and proceed before considering the intermediate sections describing the experimental technique. Attention is called to the section, Glossary of Terms.

II EXPERIMENTAL ARRANGEMENT

A. General

The external beam of the 184-inch cyclotron was steered into the cave where the target and detection equipment were located. (See Figs. 1a, 1b). The mesons, coming off at 0°, were separated magnetically from the proton beam. The mesons then passed through the copper meson energy degrader, which reduced the meson kinetic energy to approximately 21 Mev. To be counted, a meson had to pass through the two passing crystals and decay in the third or stopping crystal. This sequence was observed electronically. The electronic equipment was located outside the cave at the southeast box. The meson energy was determined by the amount of copper in the meson energy degrader.

B. Cyclotron

The scattered beam was used because it provided a better duty cycle than the electrostatically deflected beam. The scattered beam consists of approximately 350 bursts of protons, each lasting about 10^{-8} sec, and separated from each other by the cyclotron RF period, 6.6×10^{-8} sec.

The scattered beam is believed to arise from the scattering of protons on the carbon blocks protecting the dee structure. The protons were scattered into the magnetic deflector of the cyclotron and then passed through the premagnet collimator. All collimation in the horizontal plane was accomplished at this point; in the vertical plane only a partial collimation could be achieved. The final collimation in the vertical plane was carried out in the brass snout collimator at the entrance to the cave. The snout collimator is 40 inches long. The beam size was approximately 3/4 inch vertically and 1/2 inch horizontally.

C. Beam Monitoring

An absolute determination of the proton beam intensity was not necessary. Only the relative beam intensity had to be measured during a given day. The reason for not requiring absolute beam monitoring was that the efficiency of the detection system had to be determined every day be means of a standard target configuration.

Any changes in the beam monitoring efficiency from day to day were automatically compensated for as a part of the detection-efficiency correction.

The beam intensity was monitored by an Argon-CO_2 ionization chamber. The multiplication was approximately 800. The collection electrode of the ion chamber was kept at ground potential by a DC feedback amplifier. The charge was accumulated across an accurately calibrated condenser. The voltage across the condenser was measured by a Speedomax recorder with an automatic dumping arrangement.

In general the beam level was set to give a reasonable foreground-to-background counting rate. This beam level was usually of the order of 3.5×10^{-12} amperes.

D. Targets

The cross-sectional size of all targets was larger than the cross-sectional size of the beam. The target thickness for all solid targets was chosen so that the 340-Mev protons lost about 10 Mev in traversing the target. A thicker target was tried in the case of carbon but it was found that the beam level had to be correspondingly reduced to keep the background counting rate down.

The only exception to the 10-Mev limitation in thickness was allowed for the high-pressure deuterium target for run No. 5, in which case the pressure, 2000 psi, corresponded to a proton loss of 17 Mev. Run 4, which was made at pressure of 1000 psi, corresponding to a 10-Mev proton loss, showed that the shape of the spectrum would not be distorted by running at the higher pressure. The higher pressure gave a higher ratio of mesons from deuterium to mesons from the target end walls.

The high-pressure deuterium target was a modification of the target originally designed and built by R. S. White.[8] It consists of a long cylinder surrounded by a liquid-nitrogen jacket in turn enclosed in a vacuum system (see Figs. 7 and 8). The maximum operating pressure is 2,300 psi at liquid-nitrogen temperature $77^{\circ}K$. The important target specifications are: (1) 5.11 g/cm^2 of deuterium at 2,000 psi, (2) 1.78 g/cm^2 of stainless steel end walls, (3) 2-inch diameter and 24-inch length.

The B^{10} target was on loan from the USAEC. It had been prepared by electromagnetic separation.

E. Magnetic Channel Design

In order to observe mesons coming off at $0°$ to the proton beam it is necessary to separate the mesons and protons magnetically. A large pair-spectrometer magnet was used to provide the magnetic field. The gap was reduced to 3.4 inches. The cross-sectional area of the pole piece was of sufficient size so that a meson orbit of 23-inch radius could be used. The orbit turned through approximately $90°$. The meson orbits were defined by brass channeling which was designed according to the following ideas:

(a) The primary purpose of the channel is to prevent those protons from coming down the channel which have sufficient energy to penetrate the meson crystal telescope. The meson energy is not determined by the channel, but by the meson energy degrader.

(b) A meson falling within the energy range to be detected can start from any point in the target and reach any point of the crystal telescope. The size of the exit aperture of the meson channel was a compromise between the conflicting requirements of making the aperture small to shield against stray charged particles, and of making the aperture large to provide "poor geometry". The "poorer" the geometry, the smaller is the correction for multiple Coulomb scattering loss.

In order to cover the full range of meson energies, several channels were constructed. For all channels the mesons left the gap normally to the edge of the pole piece. The crystal telescope was approximately 4 inches beyond the edge of the gap. The solid targets were located well within the region of uniform magnetic field. With such a configuration, meson trajectories could be accurately drawn from magnetic field plots.

The shape of the high-pressure gas target made it necessary to locate it outside the region of uniform field as shown in Fig. 1b. A magnetic shield was used to keep the field negligibly low in the target region. Meson trajectories were traced by the wire technique. (a flexible wire carrying a suitable current and placed under the proper tension takes up the trajectory of a charged particle passing through a magnetic field). All points of the target could "see" all points of the crystal telescope.

F. Crystal Telescope, Light Pipes and Phototube

The crystal telescope consisted of 3 trans-stilbene crystals viewed by 1P21 photomultipliers through lucite light pipes. The lucite light pipes permitted removal of the phototubes to a region of a reasonably small magnetic field. In addition, the phototubes were magnetically shielded. The phototube efficiencies were essentially constant over the range of magnetic fields used in the experiment. A gamma-ray source was placed near the crystals. As the magnetic field was varied over the operating region of 14,000 - 7,000 gauss, the discriminator level had to be changed one volt in 60 to keep the singles counting rate constant.

G. Electronics

1. General block diagram and operation.

The electronics were patterned after the original design of M. Jakobson, Al Schulz, and J. Steinberger.[9] The present electronics were redesigned and built in cooperation with M. Jakobson, A. C. Schulz, and D. Hamlin (see Fig. 3).

The two channels, designated $\pi - \mu$ No. 1 and $\pi - \mu$ No. 2, following the fast coincidence, are identical. They are so arranged that background count can be taken simultaneously with the total count.

The scheme of detection is based upon the fact that the π^+-meson decays into a μ-meson. The mean life of the π^+-meson is 2.54×10^{-8} seconds.[9,10]

To be counted as a meson, an event must initiate 3 signals: two essentially simultaneous signals in crystals No. 1 and No. 2, and a third signal in crystal No. 3 that occurs during a delayed gate interval. Such an event is called a $\pi - \mu$ coincidence. A π-meson that passes through the first two crystals and decays into a μ-meson in crystal No. 3 is counted as a meson provided the $\pi - \mu$ decay occurs during the gate interval. A particle going through all three crystals is not counted as a meson because its signal in the third crystal occurs prior to the gate.

Electronically the above sequence is achieved as follows:
A coincidence ($\delta T \sim 1 \times 10^{-8}$ sec.) is required in crystal 1 and 2 by
the fast coincidence circuit. This coincidence triggers the gate
generator, which produces a voltage gate starting 2.2×10^{-8} seconds
after the fast coincidence and lasting 10^{-7} seconds. The signal from
the third phototube is put in coincidence with the gate. The proper
timing is achieved by the use of suitable lengths of RG 63-U cable
between units. In order to obtain workable voltage levels, several
distributed amplifiers have been introduced.

The short-delay operation, in which the gate starts 2.2×10^{-8}
seconds after the fast coincidence, permits accidental events, also,
to be counted as mesons. For example a knock-on proton may pass
through the first two crystals and a second knock-on proton may
pass through the third crystal during the gate interval. The
accidental counting rate can be measured in a long-delay operation,
in which the gate (though still of the same duration) is delayed
19×10^{-8} sec. after the fast coincidence. By this time any meson
that could have tripped the fast coincidence will have decayed and
therefore all counts are accidental. The true meson count is given
by the difference between the short-delay count and the long-delay
count.

For any given measurement, $\pi - \mu$ channel No. 1 is operated
on long delay while $\pi - \mu$ channel No. 2 is operated on short delay,
the delays are then interchanged for the same amount of integrated
proton beam. The primary advantage of this mode of operation is
that fluctuations in the accidental counting rate caused by beam-
intensity fluctuations are canceled out. If the beam intensity
suddenly increases during a measurement the accidental rate in-
creases equally for both the short-delay and long-delay counts.
The net or true meson count is unaffected.

The meson and gate output are fed to standard UCRL linear
amplifiers and then to scalers.

2. **Fast coincidence chassis.**

This unit is built on one chassis (Fig. 4). It consists of two separate distributed amplifiers A and B and a distributed coincidence of the type designed by Dr. C. Wiegand.[11] The distributed amplifiers have a measured gain of about 40 and calculated band width of 175 megacycles. With a 1/4-volt input the output is 10 volts. With a 1/8-volt input to amplifiers A and B the coincidence output is 4 volts. With 1/8-volt input to one amplifier the output of the coincidence is 0.4 volts.

3. **$\pi - \mu$ chassis.**

The $\pi - \mu$ chassis consist of: π-amplifier, gate generator, μ amplifier, $\pi - \mu$ coincidence, output discriminator (Fig. 5). The gate generator is a cathode coupled univibrator which also acts as a discriminator. It is fired by a 6-volt pulse lasting ~10^{-8} sec. The gate amplitude is approximately 10 volts and lasts ~10^{-7} sec. The tubes for the gate generator must be selected for satisfactory length, amplitude, and shape of gate. In general the 6AN5 must have a high transconductance.

4. **Critical grid biases and voltages.**

There are several critical grid levels whose action must be understood. G_1 of the $\pi - \mu$ coincidence controls the level of the μ signal to make a $\pi - \mu$ coincidence. High voltage No. 3 controls the level of the μ signal input to both $\pi - \mu$ chassis. The π amplifier bias determines the level of the signal required to fire the gate generator.

III EXPERIMENTAL PROCEDURE

A. Original Setting of Phototube Voltages and Bias Levels

1. High-voltage plateuas for phototubes No. 1 and No. 2.

First the gate counting rate for each π - μ chassis was equalized by adjusting the π amplifier bias, which sets the level of signal from the fast coincidence required to fire the gate generator.

Plateaus for HV No. 1 and No. 2 were obtained for meson counting rates (Fig. 6). HV No. 1 and No. 2 were set to 1,200 volts.

2. Lack of plateaus for phototube No. 3.

It had been hoped that a plateau for HV No. 3 might be obtained because the μ meson has a fixed kinetic energy of 4.2 Mev. Extensive exploration failed to reveal any such clear-cut plateau. There was a region of reasonable slope, but it was followed by an increasing slope with no clear distinction between the two regions. In fact, at the highest setting of HV No. 3, the counting rate exceeded the rate calculated for 100% efficiency of the crystal telescope. Three problems immediately arose:

(a) why is there no plateau and why does the counting rate increase indefinitely?

(b) what is a reasonable setting for HV No. 3?

(c) how can the counting efficiency be determined?

For the first pair of questions, a number of factors may have contributed. The range of a 4.2-Mev μ-meson is 1.2 mm in the trans-stilbene and is to be compared with the 8.8-mm thickness of the third crystal. At best any observed plateua would therefore have a finite slope. The light-collection efficiency can vary over different portions of the crystal. Further, long light pipes cause greater statistical fluctuations in phototube pulse height.[12] In addition, knock-on protons arising from the general neutron background can cause large pulses in the crystal telescope. If HV No. 3 is increased, these pulses may saturate the distributed amplifiers and broaden the pulses sufficiently so that the tail of the broadened pulse falls into the short-delay gate starting 2.2×10^{-8} sec. later. The long-delay gate, of course, would not be sensitive to such an event, because the broadened pulse would have disappeared. Such an effect could account for the indefinite increase of meson counting rate.

The question of where to set HV No. 3 was settled as follows: A thick polyethylene target was used to produce a large number of π^+-mesons from the reaction $p + p \rightarrow D + \pi^+$. The magnetic field was set for the kinetic energy of these mesons, 62 Mev. The meson energy degraders which normally would have slowed these mesons to 21 Mev were removed. This allowed a large number of high-energy mesons and protons to penetrate the crystal telescope. Except for mesons scattered off the walls of the channel, there should have been no 21-Mev mesons coming down the channel. Hence most pions should have passed right through the telescope before decaying. The counting rate was then measured as a function of HV No. 3. The counting rate was observed to increase slowly and then suddenly increase rapidly at about 1400 volts. The counting rate below the break was consistent with the number of mesons that might scatter from the channel walls. The operating voltage was set below the break at an arbitrary value of 1300 volts. This procedure was admittedly ad hoc. The justification is discussed under "Validity of Detection" in the next sub-section.

As for the problem of determining the counting efficiency, a standard target configuration was used.

B. Validity of Detection.

The criterion for setting HV No. 3 provided no proof that only mesons were being counted. To further justify the setting of HV No. 3 a number of tests were made.

In the first place a half-life for the π meson was determined by varying the gate delay. The value so obtained agreed with previous measurement.[9, 10]

The π^+ spike in the reaction $p + p \rightarrow D + \pi^+$ was clearly observed in a CH_2-carbon subtraction experiment. Furthermore the CH_2-carbon difference was statistically zero above the π^+ spike.[13a, b]

The ratio of hydrogen yield of π^+ to the carbon yield agreed with nuclear plate data.

The carbon spectra measured at 0° and 90° agreed with the spectra obtained by plate data.[14, 15]

From deuterium no mesons were observed above the maximum energy allowed by kinematics.

It seems reasonable to conclude that the equipment counted only mesons within the statistics so far obtained, which are of the order of 5 to 10 percent. It is possible that there may be a 5 percent background, for example saturation proton pulses, which was counted with the true meson count.

C. Setup Procedure.

At the beginning of each run the standard target configuration was set up. HV No. 3, G_1 for $\pi - \mu$ No. 1 and G_1 for $\pi - \mu$ No. 2 were adjusted so that

(a) Both $\pi - \mu$ No. 1 and $\pi - \mu$ No. 2 counted within 20 percent of the same rate.

(b) The over-all counting rate agreed with 20 percent of the standard rate.

The beam level was set so that the net meson count was at least equal to or greater than the background rate.

D. Efficiency Control.

The maintenance of counting efficiency was critical. The significant grid biases were monitored approximately every 5 hours. HV No. 3 was controlled to within 3 volts at all times by means of an electrostatic voltmeter. With these precautions the efficiency was never observed to change during a given day, although it did shift from day to day. By appropriate cycling of targets and meson energies during each day any efficiency changes could have been detected. The actual counting efficiency from day to day and from run to run was measured by the standard targets or by other repeated target conditions. (See subsection, Normalization of Data from Day to Day)

E. Absolute Detection Efficiency.

The absolute detection efficiency was calculated from absolute cross sections, derived from nuclear emulsion data. The efficiency was approximately 13 percent, that is, only 13 percent of the mesons decaying in the stopping crystal were counted. It should be noted, 60 percent of the mesons decay prior to the start of the gate. It the system had been 100 percent efficient only 40 percent of the mesons decaying in the third crystal could have been counted anyway. The decrease from 40 percent ot 13 percent is the measure of efficiency of the system of crystals, light pipes, phototubes, etc.

IV. DATA REDUCTION

A. General

The direct experimental data consisted of net meson counts per unit of integrated beam intensity. Three steps were required to obtain absolute differential cross sections.

Step 1. Normalization. The relative counting efficiency was measured and the data were normalized accordingly. The deuterium data presented a special problem.

Step 2. Corrections. 1) Decay in flight, 2) Multiple Coulomb scattering losses, 3) Variation of energy resolution of detector, 4) Meson and proton attenuation losses in the target and meson-energy degraders.

Step 3. Transformation from relative to absolute cross sections. Actually, relative cross sections were measured. Absolute cross sections were determined by comparison with carbon data, for which Dudziak has measured the absolute cross section by nuclear emulsion techniques. [15] See subsection IV E, Errors for Dudziak's data, used in this analysis.

More specifically the direct experimental data consisted of:

S_1 = short-delay count from $\pi - \mu$ No. 1
L_1 = long-delay count from $\pi - \mu$ No. 1
S_2 = short-delay count from $\pi - \mu$ No. 2
L_2 = long-delay count from $\pi - \mu$ No. 2

The above were combined to yield:

$$\text{Net count} = S_1 + S_2 - L_1 - L_2 \pm \sqrt{S_1 + S_2 + L_1 + L_2}$$

B. Normalization of Data from Day to Day

Shifts in counting efficiency were determined as follows. Consider two days, A and B, in which identical points (1), (2), (3) etc. are measured.

Experimental points	Observed net meson counting rate Day A	Day B
(1)	n_1	N_1
(2)	n_2	N_2
(3)	n_3	N_3
⋮	⋮	⋮
(i)	n_i	N_i

Assume: Efficiency Day A = 1

Efficiency Day B = k

Then aside from statistical fluctuation

(n_1) (k) should equal N_1

(n_2) (k) should equal N_2 etc.

By least squares the function $\sum_i (n_i k - N_i)^2$ is minimized as a function of k.

The value of k usually lay between 0.85 and 1.15. A standard deviation for k was also calculated. Frequently such calculations gave a value $k = 1.10 \pm 0.10$ so that it was debatable whether k was statistically different from 1. Whether 1 or 1.1 is used makes little difference, because all points of a spectrum were covered during each day; the shape of the spectrum would not be affected regardless of whether k was set to 1 or 1.1. The only exception was run No. 4.

In this fashion a given run was internally normalized; that is, the data from different days of a given run were normalized together. Then different runs were normalized together in the same way. The normalization of the deuterium gas data, discussed in the following subsection, was more complicated because two different gas pressures were used.

C. Normalization of Deuterium Data

Runs 5 and 6 were each normalized internally first. The data at this point could not be combined because run No. 5 was made at 1,000 psi and run No. 6 was made at 2,000 psi. Proton and meson attenuation factors were different for the two runs. The mean proton and meson energies were different in the two cases by virtue of the difference in energy loss by ionization in the target.

Proton attenuation in the deuteriums was calculated using a total interaction cross section of 58 mb. This cross section was estimated. Experimental data at 400 Mev and at 90 Mev indicated that the total interaction cross section for protons on deuterium could be adequately calculated by taking the sum of the total interaction for protons on protons plus the total interaction for neutrons on protons. The same procedure was assumed to be valid for 340-Mev protons.

Energy	Process	Total interaction
400 Mev	P + P	24 mb measured[16]
	P + N	33 mb measured[17]
		57 mb sum of above
	P + D	55.6 measured[16]
90	P + P	24 mb measured[18]
	P + N	76 mb measured[19]
		100 mb sum of above
	P + D	92 ± 7 measured[20]
	N + D	117 ± 5 measured[21]
340	P + P	24 measured[18]
	P + N	34 measured mean of 260 Mev[22] and 400 Mev[17]
	P + D	58 sum of above

The cross section for the attenuation of mesons in deuterium was taken to be 110 mb. This is the average of

$$36 \text{ mb for } T_\pi = 60 \text{ Mev}[23]$$

$$190 \text{ mb for } T_\pi = 140 \text{ Mev}[24, 25]$$

The multiplication factor for correcting run No. 5 to run No. 6 for both meson and proton attenuation was 0.94 (that is, run No. 5 corrected to run No. 6 = 0.94 · run No. 5).

The mean proton energy was different for the two targets. The difference in excitation was estimated in two ways. The first was to assume the excitation would be the same as that for the $P + P \rightarrow D + \pi^+$ measured by Schulz,[13a, b]. This calculation gave a correction factor of 0.90 for run No. 5. The second estimate was determined by calculating the normalization factor required to bring the two spectra into agreement after all other corrections had been made. This calculation gave a correction factor of 0.86. The 0.86 correction was used.

The π^+-spectrum was appropriately shifted along the T_π axis to account for the difference in mean meson energy in the target for runs No. 5 and No. 6.

Lastly the difference in the number of nuclei/cm^2 was accounted for.

With the above correction run No. 5 was normalized to run No. 6. A smooth curve was then run through all the points by eye. (See Fig. 13. Note all corrections have been applied.)

To a first approximation the net deuterium contribution course is given by the target full-target empty difference. But it is not so simple as this. When the target is full, the number of mesons produced in the end walls is less then when the target is empty. Mesons produced in the front end wall are attenuated in passing through the deuterium. At the same time, the number of mesons produced in the rear end walls of a full target is smaller because the proton beam is attenuated by nuclear interactions with the deuterium, and the protons themselves lose energy in ionizing deuterium. Thus the correction for target-empty conditions is not so great as might at first be expected.

Appropriate cross sections previously discussed were used to calculate the above attenuation effect. It was assumed that the excitation for steel would be the same as the excitation measured by D. Hamlin[14] for carbon at 90°. In total the net target-empty counting rate was multiplied by 0.68 to account for the effects of the proton attenuation and degradation in energy, plus meson attenuation. A smooth curve was run through the points by eye. See Fig. 13.

The net deuterium difference was then read off the graph to give the relative π^{+} yield as a function of meson kinetic energy.

The absolute deuterium cross section was determined by measuring the yield from a carbon target relative to the deuterium yield and using the absolute carbon cross section measured by W. Dudziak.[15] The carbon target consisted of six slices of carbon spread out to simulate the geometry and thickness, in terms of proton energy loss, of the gas target. Corrections were made for proton absorption in carbon based on the total interaction cross section measured by Kirschbaum[26] and for meson absorption based on nuclear area.

D. Corrections

    1. Introduction.

The data now having been normalized to compensate for shifts in detection efficiency, it remains to apply a number of corrections to obtain the true relative value of $d^{2}\sigma/dE\,d\Omega$. All these corrections are a function of the meson kinetic energy. The corrections are:

(a) Variation of energy resolution of detector.

(b) Loss of mesons due to multiple Coulomb scattering of mesons out of the crystal telescope.

(c) Meson loss due to nuclear interactions in the meson energy degraders.

(d) Decay of mesons in flight.

Except for run No. 6, Series IV, the attenuation of protons and mesons in the target was negligible. For this run see the subsection IV C, Normalization of Deuterium Data for a full discussion of the correction made.

2. Energy Resolution of Detector.

The crystal telescope detects mesons whose kinetic energy is 21 ± 2.5 Mev. Copper meson-energy degraders were used to degrade the higher energy mesons so that they could be detected. The range-energy relations are such that the effective energy resolution is compressed as higher energy mesons are observed. The energy of a meson may be expressed as the range, in g/cm^2 of material required to stop it.

$$E = E(R) \qquad \qquad E = \text{kinetic energy of meson}$$
$$R = \text{range in } g/cm^2$$

$$E_o = E(R_o) = 21 \text{ Mev.} \quad \text{Mean detection energy with no meson}$$
$$\text{energy degrader}$$

$$R_o = \text{range in copper corresponding}$$
$$\text{to } E_o$$

Suppose an amount of copper R is placed in front of the detector

$$E_R = E(R_o + R) \qquad \qquad E_R \text{ is the mean energy of meson}$$
$$\text{that will be detected if } R \text{ } gm/cm^2$$
$$\text{are placed in front of the crystals}$$

Actually the detector will detect mesons in a range of energy $\pm \Delta E_o$ about E_o. For no copper

$$E_o \pm \Delta E_o = 21 \pm 2.5 \text{ Mev}$$
$$= E(R_o \pm \Delta R_o) \qquad \Delta R_o \text{ is determined by } \Delta E_o$$
$$= E(R_o) \pm \left[\frac{dE}{dR} \right)_{R_o} \right] \left[\Delta R_o \right]$$

$$\Delta E_o = \left[\left(\frac{dE}{dR} \right)_{R_o} \right] \left[\Delta R_o \right]$$

If R gms/cm^2 of copper are now added,

$$E_R + \Delta E_R = E(R_o + R + \Delta R_o)$$

$$\Delta E_R = \left[\frac{dE}{dR}\right)_{R_o+R}\right]\left[\Delta R_o\right]$$

Therefore $\quad \dfrac{\Delta E_o}{\Delta E_R} = \left[\dfrac{dE}{dR}\right\}_{R_o}\right] \Big/ \left[\dfrac{dE}{dR}\right\}_{R_o+R}\right]$

ΔE_R is the effective energy resolution corresponding to the meson energy $E_R = E(R_o + R)$.

3. Meson Loss Due to Nuclear Interactions in Meson Energy
    Degraders.

The interaction cross section for loss of mesons in the meson energy degraders was taken as a constant given by nuclear area

$$\sigma(\text{geometric}) = \pi\,(1.40\,A^{1/3})^2 \times 10^{-26}\ cm^2$$

There are two types of nuclear interactions in the copper meson-energy degraders which can result in the loss of mesons. The predominant loss comes from inelastic nuclear scattering. The second mode of loss is diffraction scattering, which can scatter mesons out of the crystal telescope. D. H. Stork's[27] data were used to calculate σ(inelastic.)

The loss from σ(diffraction) can be estimated by comparison with the loss of multiple Coulomb scattering which is calculated later. Roughly speaking, the angular distribution is the same for diffraction scattering and multiple Coulomb scattering. For equal half angles, the loss should be the same in both cases. The σ(geometric) gives the effective total loss of mesons due to diffraction and inelastic scattering to within 10 percent for mesons whose energies are in the range 50-150 Mev. Below 50 Mev the error in using σ(geometric) may become as much as 30 percent but the total correction is less than 15 percent. The error in the total correction is of the order of 5 percent in this case. Specifically the number of pions lost is given by

$$I = I_o\, e^{-N\sigma/M}$$

I_o = intensity of incident pions

I = intensity of pions getting through

N = number of nuclei/cm^2

σ = cross section

4. Multiple Coulomb Scattering Loss.

Due to multiple Coulomb scattering in the meson energy de-grader, some mesons are scattered out of the stopping crystal. See Appendix I for the details of the calculation. The method of Eyges[28] is followed to calculate the correction. Very briefly, he derives a distribution function that includes the effect of energy loss of the scattered particle as it passes through material.

F (t, y, θ) = distribution function

t = distance traveled through material measured in radiation lengths

θ = angle between direction of incident particle and final direction of travel projected on to and any plane containing the original direction of travel

θ = distance measured perpendicular to original direction of travel and projected on the same plane as for θ.

The third stopping crystal was then divided into a number of zones. By means of the distribution function F (t, y, θ) the number of mesons lost to each zone was calculated. The losses in all the zones were numerically integrated to give the total loss.

5. Decay in Flight.

A correction must be made for mesons lost by decay in flight. The proper time elapsed in the meson frame is

$$d\tau = \frac{dt}{\gamma}$$

$$= \frac{ds}{v\gamma}$$

$$= \frac{M_o}{P} ds$$

$$\int d\tau = \int \frac{M_o}{P} ds$$

d τ = proper time

dt = lab. time

$\gamma = 1/\sqrt{1 - B^2}$

ds = distance

v = velocity of meson

M_o = rest mass

P = meson relativistic momentum

By numerical integration of the above expression of the range energy curves for copper[29] and trans-stilbene it can be shown that the loss of mesons by decay in the copper absorber and the first two crystals is negligible. The fraction of mesons decaying in flight between the target and crystal telescope is calculated. In the case of the deuterium gas target, the target was divided into 4 zones and the correction calculated for each zone.

The value used for the mean life at the π^+-meson was 2.54×10^{-8} seconds[9, 10].

Typical values for the corrections are given in the following table. For a given T_π the total correction is the product of the individual corrections. The normalized data are multiplied by the total correction to give the corrected relative $d^2\sigma/dE\,d\Omega$.

Table

T_π Channel	Energy Resolution	Meson loss in Meson Energy Degraders	Decay in Flight	Multiple Coulomb Scattering Loss
35	1.36	1.04	1.19	1.10
45.8	1.06	1.08	1.16	1.13
64.5	1.90	1.17	1.13	1.11
83.8	2.09	1.29	1.11	1.15
106.2	2.26	1.45	1.10	1.21
124.9	2.34	1.61	1.09	1.26
143	2.39	1.79	1.08	1.29

E. Errors

The errors shown in all cases are the statistical errors arising from counting. The errors are expressed in standard deviations. For a given meson energy the errors of the relative cross sections should be correctly given by the statistical counting errors because all the correction factors are fixed for a given meson energy. The comparison of differential cross sections at different meson energies is another matter. In this case there may be systematic errors in the correction for multiple coulomb scattering losses and for meson loss due to nuclear interactions in the copper meson-energy degraders. It is estimated that the systematic error of these corrections is not greater than:

	Estimated Maximum Systematic Error in the Correction Factor		
Meson Energy	65 Mev	105	145
Meson Nuclear interactions in meson energy degraders	5%	10%	15%
Multiple Coulomb scattering losses	2%	4%	6%

The absolute values assigned to the production cross section are normalized to W. Dudziak's[15] nuclear emulsion analysis of the reaction

$$P + C \rightarrow \pi^+ + A'$$
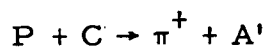
Thus any absolute error in his measurements appear also in the absolute values given here; the ratios, however, are still valid no matter what absolute values they are derived from. His experimental values are

T Mev	$d^2 \sigma /dE \, d\Omega \times 10^{-30} \, cm^2 \, Mev^{-1} \, steradian^{-1}$
56	12.16 ± 0.92
72	15.71 ± 0.93
90.1	20.77 ± 1.33

V RESULTS AND INTERPRETATION

A. General

The results of this experiment and of related work are summarized in the following tables and figures.

Experiment/targets	Type of cross section	T_π Mev	Meson angle to beam	Table	Figure
Series I[5] C, Al, Cu, Fe, Ag, Pb	$d^2\sigma/dE\ d\Omega$	= 53	0°	1	9
Series II Be[9], B[10], B[11], C[12]	$d^2\sigma/dE\ d\Omega$ $d\sigma/d\Omega$	34, 51, 69, 88, 110, 129	0°	2	9
Series III C, Cu, Pb	$d^2\sigma/dE\ d\Omega$ $d\sigma/d\Omega$	52, 88, 147	0°	3	10, 11 9
Series IV Deuterium	$d^2\sigma/dE\ d\Omega_2$ $d\sigma/d\Omega$	40-140	0°	4, 5	14, 13 9
D. Clark[3b] Be, C, Al, Cu, Ag, W, Pb	$d^2\sigma/dE\ d\Omega$	40	140°		9
Block[6] C, Cu, Pb	$d^2\sigma/dE\ d\Omega_2$ $d\sigma/d\Omega$	Complete spectra	90°		9
Sagane[7b] Be, C, Al, Cu, Ag, Pb	$d^2\sigma/dE\ d\Omega$	33	90°		9

Figure 9 gives a general summary of experimental work on nucleon production of pions. Note it is the shape of the curves, not the absolute ordinate, which is important. In several cases the absolute ordinate is arbitrary. In Fig. 9 the differential cross sections, $d^2\sigma/dE\ d\Omega$, of Series II and III, and of Block, Passman, and Havens have been integrated over meson energy. This procedure seems reasonable because the A dependence of the differential cross section is weakly dependent on meson energy (see Fig. 10). The only startling discrepancy is Clark's Be point, which seems unreasonably low. Otherwise the general trend is similar within statistics for all experiments.

The data of Series I indicated a smooth variation of meson yield as a function of atomic number. The same conclusion was borne out by the work of others (See Fig. 9). The data of Series II implied

that the yield of mesons did not alter radically between neighboring
isotopes. It was decided, therefore, to reduce the number of elements
and meson energies observed in order to achieve better statistics.
In Series III the yield was measured from only C, Cu, and Pb and for
only the three meson energies 52, 88, and 147 Mev.

The deuterium spectrum of Series IV is exhibited in Fig. 14.
Within statistics the curve agrees with the maximum kinetic energy
allowed by kinematics, 136 Mev. The curve was located by eye to give
the best fit to the data irrespective of the 136-Mev cutoff. The curve,
as drawn, cuts off at a slightly higher energy than 136 Mev. The curve
of Fig. 14 is the difference between the two curves exhibited in Fig. 13:
target full and target empty.

B. Model for Complex Nuclei, C, Cu, and Pb

The data of Series III can be interpreted by means of the fol-
lowing nuclear model, which, though crude, is adequate:

(a) The nucleus is considered to consist of free nucleons
having an appropriate momentum distribution. This momentum distri-
bution, whatever it may be, is taken to be the same for C, Cu, and
Pb. For a specific incident-proton energy the production of mesons
within the nucleus should therefore be the same in C, Cu, and Pb except
for the differences in the numbers of protons and neutrons. Exclusion
effects on final-state nucleons are neglected. The qualitative effect
of considering exclusion effects should be to enhance the production
in the higher-Z elements relative to the lower-z elements, because
there is a higher density of excited states for the higher-Z nuclei.

(b) Mesons are produced solely in collisions between
the bombarding proton and protons within the nucleus. Proton-neutron
collisions are ignored in the production of π^+-mesons. The justification
for this neglect of P + N collisions is the large π^+/π^- production ratio
observed in proton bombardment of carbon[6,15] in which both P + P
and P + N collisions occur. If relatively few π^- are produced in P + N
collision it is reasonable to assume by symmetry that very few π^+ will
be produced in these same P + N collisions. The large π^+/π^- ratio
therefore implies a large ratio of π^+ produced in P + P collisions com-
pared to P + N collisions. The production of π^+ within the nucleus
should therefore be proportional to the number of protons, Z.

(c) Some mesons produced within the nucleus are reabsorbed; $\lambda_m \equiv$ meson mean free path for absorption.

(d) Bombarding protons are attenuated by competing processes as the protons pass through the nucleus; $\lambda_p \equiv$ mean free path for proton absorption by competing processes in nuclear matter.

(e) Elastic scattering of mesons within the nucleus is ignored.

(f) Coulomb barrier effects are considered negligible.
An attenuation factor F was calculated such that

$$F = \frac{\text{Actual meson yield with proton and meson attenuation}}{\text{Hypothetical meson yield for no attenuation of protons and mesons}}$$

See Appendix II for details of the calculation of F. The production cross section is expected to vary as

$$\text{yield} \sim (Z)(F)$$

The problem in calculating F was to assign the proton and meson mean free paths λ_p and λ_m respectively.

Three sets of λ_p were considered:

C	Cu	Pb	Set
3.6	3.6	3.6×10^{-13} cm	1
4	6.25	8.3	2
4	5	6	3

Set 1 was used by R. Hales[30] in his analysis of the yield of π^0 mesons from proton bombardment as a function of atomic numbers. The value 3.6×10^{-13} cm is based on taking the average of the experimental value for elastic scattering cross section for P + P and N + P collisions.

Set 2 is based on the experimental results of A. Kirschbaum[26] who measured the total attenuation cross section for 340-Mev protons on C, Cu, and Pb, from which he was able to calculate a mean free path for protons in nuclear matter. His mean free paths are expected to be too large because he counted all protons falling within the energy range 320 to 340 Mev as being unattenuated. As a matter of fact a 320-Mev proton would have suffered a slight nuclear interaction. A 320-Mev

proton is less effective in producing mesons than a 340-Mev proton and, for calculating λ_p, should be considered as having had a nuclear interaction. Stated in other words, if Kirschbaum had counted only those protons falling within the range of, say 335 to 340 Mev, his calculated λ_p would have been smaller and more realistic for the purposes of this analysis.

Set 3 of λ_p is arbitrarily chosen to fall between sets 1 and 2. When combined with a reasonable λ_m, the data are better fitted by the λ_p of set 3 than by the other two sets of λ_p.

A single set of values for the meson mean free path in nuclear matter was taken from D. H. Stork's thesis[27]. He determined a best value for λ_m as a function of meson kinetic energy. His analysis included all π^+ scattering data available as well as his own measurements.

T_π	λ_m
52	7.0×10^{-13} cm
88	2.8
147	1.1

In Fig. 12 $(d^2\sigma/dE\,d\Omega)/ZF$ is exhibited. F is calculated using Stork's λ_m and the λ_p of set 3. The points should lie on a horizontal line.

The π^+ yield is consistent with the chosen values of λ_p and λ_m. It should be emphasized, however, that the data could also be fitted with other sets of λ_p and λ_m in which λ_p is increased and λ_m decreased, or vice versa.

C. Interpretation of λ_m

It is possible to interpret λ_m in terms of the scattering cross sections of π^+ and π^--mesons on protons. As a π^+-meson passes through a carbon nucleus and interacts with individual nucleons, several processes may take place:

(a) $\pi^+ + p \rightarrow \pi^+ + p$ elastic

(b) $\pi^+ + N \rightarrow p + \pi^o$ charge exchange

(c) $\pi^+ + N \rightarrow N + \pi^+$ elastic

(d) $\pi^+ + N \rightarrow p + \gamma$ inelastic

Reaction (a) has been observed as a function of angle for T_π = 53, 78, 110, and 135 Mev.[25] As a first approximation one might assume that any meson scattered through an angle greater than 90° is lost with

respect to production at 0°. About 68 percent of the mesons in the energy range 53 to 135 Mev are scattered through an angle greater than 90° for process (a)[25] (note that center-of-mass values were taken as equal to the laboratory values). The 68-percent factor has been applied to σ (a) values taken from a number of experiments[23,25,32-34] to determine the loss by process (a).

The next three processes, (b), (c), and (d), must now be considered. By the assumption of charge independence of nuclear force one can say that processes (b), (c), and (d) should be equivalent to the following processes which have been observed experimentally:

(b') $\pi^- + p \rightarrow N + \pi^o$

(c') $\pi^- + p \rightarrow p + \pi^-$

(d') $\pi^- + p \rightarrow N + \gamma$
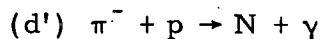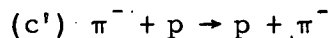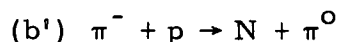
Process (d') can be shown to be negligible by a detailed balance argument from the inverse reaction[25].

In process (c') the mesons are scattered predominantly forward[25] and are not lost. Of the three processes, (b'), (c'), and (d'), process (b') is the primary process for losing mesons. Unfortunately to date (b') has not been directly observed except for two meson energies, T_π = 120 and 140 Mev.[25] For these two energies

$$\sigma \ (b') \cong 2 \ \sigma \ (c')$$

Furthermore, the sum of cross sections for (b') and (c') agrees with total attenuation cross section measurements.[25] A rough measure of (b') at other T_π can therefore be estimated by taking 2/3 of the total attenuation cross section of π^- on protons. The total attenuation cross section has been measured for T_π = 60 Mev[23], 89 Mev and 112 Mev[35]. With these values it is possible to calculate

$$\sigma \ (b') = 2/3 \ \sigma \ (\text{total attenuation})$$

Combining results,
$$\sigma \ (\text{total absorb}) = \sigma \ (\text{total, b'}) + \int_{90}^{180} \frac{d\sigma}{d\Omega} \ (a) \ d\Omega$$

$$= 2/3 \ \sigma \ (\text{total attenuation}) \pm 0.68 \ \sigma \ (a)$$

In the following table the factors Z/A and (A - Z)/A give the relative number of protons and neutrons in the carbon nucleus. From

the σ (total absorption) it is possible to calculate the mean free path, λ (calc), which is to be compared with λ_m, Stork's experimental value.[27]

T_π Mev	52	88	147
$(Z/A)\ 2/3\ \sigma(a)$	6.1×10^{-28} cm^2	18.5	55
$\frac{A-Z}{A}$ (.68) σ(total attenuation)	6.0×10^{-28} cm^2	7.0	17
σ(total absorption)	12.1×10^{-28} cm^2	25.5	72
λ(calc.)	8.9×10^{-13} cm^2	4.2	1.5
λ_m (Stork)	7.0×10^{-13} cm^2	2.8	1.1

The agreement between the last two lines is rough. It would appear that λ_m can be interpreted in terms of the observed interaction cross section of mesons with nucleons. Some caution is required because the λ for the mesons under consideration is not short compared to the inter-nucleon distance, 2.8×10^{-13} cm. For π-mesons:

$$T_\pi = 45 \qquad 85 \qquad 150 \text{ Mev}$$
$$\lambda = 1.59 \qquad 1.1 \qquad 0.76 \times 159 \times 10^{-13}$$

($\lambda \equiv$ de Broglie wave length/2π)

The above approach may explain the discrepancy observed by S. Leonard,[36] who measured the differential production cross section at 180° for the reaction

$$P + C \to \pi^+ + A'$$
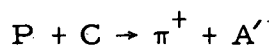
His observed yields were 4 to 30 times larger than his calculated yields, depending upon his assumptions for the internal momentum distribution for nucleons in carbon and the excitation function for the reaction $P + P \to \pi^+ + A$. The ratio for π^+ yields at 0° and 180° from $P + C \to \pi^+$ is

$$\frac{d\sigma\ (0°)/d\Omega}{d\sigma\ (180°)/d\Omega} = \frac{21}{1.77} = 11.9$$

It would take a small amount of backscattering of mesons produced at 0° to augment the yield at 180° by a factor of 4 to 10. Specifically the yield at 180° could be increased from 1.7/4 to 1.7 by a backscattering of $\frac{(3/4)(1.7)}{21}$ = 6 percent of the 0° mesons. The mean free path for elastic backscattering of mesons is not inconsistent with this percentage.

D. Calculation of Total Production Cross Section for Carbon

The $d\sigma/d\Omega$ has been measured for $P + C \to \pi^+ + A$ at the three angles

θ	$d\sigma/d\Omega$	Reference
$0°$	21.0×10^{-28} cm^2/steradian	15
$90°$	3.35	15
$180°$	1.77	36

From these data it is possible to calculate the total cross section experimentally observed.

Theoretically, the yield from carbon can be calculated with the following assumptions:

(a) The production arises from only p + p collisions within the carbon nucleus.

(b) The internal momentum distribution within the carbon nucleus is given by a gaussian function such that the probability falls to 1/e for a nucleon of energy 16 Mev. Such a distribution is suggested by the work of Cladis[37] on the energy spectrum of protons scattered from carbon.

(c) Two excitation functions were tried, $T_\pi^{3/2}$ and T_π^2. The data of Schulz[13a, b] and Durbin, Loar, and Steinberger[38] were fitted by the two forms of the excitation function. The $T^{3/2}$ excitation is the energy dependence predicted by PS theory with PV coupling. The T_π^2 excitation gives a better fit to the experimental data of Passman, Block and Havens,[39] who observed the excitation for $P + P \rightarrow D + \pi^+$ at $90°$.

(d) The angular distribution measured by Stevenson[40] was used for the angular integration.

(e) Thirty percent was added to the π^+ yield for non-deuteron formation.[41]

$$P + P \rightarrow P + N + \pi^+$$

The total production of mesons within the nucleus was calculated in three steps: (i) transformation to the center-of-mass system for the incident proton and particular nucleon, (ii) calculation of the energy available, (iii) and determination of yield by the excitation function. Next the effect of attenuation of protons and mesons was estimated in a manner similar to the calculation in Appendix II.

The results of the calculation are summarized:

Excitation function	T_π^2	$T_\pi^{3/2}$
Calculated relative cross section per proton (compared to hydrogen = 1) in carbon, no attenuation of protons and mesons	8.3	3.8
Calculated relative cross section per proton (compared to hydrogen = 1) with proton and meson attenuation	2.7	1.2
Experimental relative cross section per proton (compared to hydrogen = 1)	2.7	2.7

The above calculation is uncertain for a number of reasons. The excitation function is being extrapolated far beyond experimental values. The internal-momentum distribution is uncertain for the high-momentum components. The model may be bad. A number of rough estimates were made. The remarkable fact is that the calculated and observed total cross section per proton are of the same order of magnitude.

VI CONCLUSIONS

1. The yield of π^+ mesons is a smooth function of atomic number.

2. No special isotope effects were observed for the π^+-meson yield from Be^9, B^{10}, B(natural) and C^{12}.

3. The yield as a function of atomic number can be explained in terms of

(a) Production of π^+ only from P + P collisions

(b) Attenuation of mesons and protons with reasonable mean free paths given by

T_π	Meson Mean Free Path λ_m
55 Mev	7×10^{-13} cm
85 Mev	2.8×10^{-13} cm
145 Mev	1.1×10^{-13} cm

Element	Proton Mean Free Path λ_p
C	4×10^{-13} cm
Cu	5×10^{-13} cm
Pb	6×10^{-13} cm

4. The experimental values for λ_m can be interpreted in terms of the observed interaction cross sections between mesons and free protons. Furthermore λ_m is of the right order of magnitude to account for sufficient attenuation of mesons to explain the total production cross section for π^+-mesons produced by proton bombardment of carbon.

ACKNOWLEDGMENTS

The achievement of this experiment may be attributed to the skills and efforts of many, whose generous cooperation was inspiring and helpful.

Professor Chaim Richman guided and stimulated the work by innumerable conversations. He was generous with his time, and provided that fresh or balanced point of view as necessary.

Mr. Dan Hamlin, from beginning to end, was the indispensable teammate who helped see the job through in all details, from questions of fundamental design and interpretation to sweating it out until four A. M. when necessary on cyclotron runs.

In considerable part the design and construction of the electronic equipment was undertaken by Drs. Mark Jakobson and Alvin Schulz. They assisted in obtaining the data of Series I and II.

After several false starts the high-pressure target was finally made to work by the preservering efforts of R. A. Byrns for general guidance, John Wood for the redesign which worked, Bob Scott and Don Bliss for enterprising cooperation and skill in fabrication of the target.

Dr. Steve White and Gordon Repp assisted during the course of several cyclotron runs.

Mr. James Vale and the cyclotron crew always went out of their way to comply with the requests of the experimenter even when those request bordered on the unreasonable.

And to Diana Merritt, whose encouragement and support on the home front continued through the inevitable ups and downs of any experiment I am incalculably indebted.

GLOSSARY OF TERMS

Equipment and Operating Terms

Crystal Telescope--consists of crystals No. 1, No. 2 and No. 3

Passing Crystals--crystals No. 1 and No. 2

Stopping Crystal--crystal No. 3

Meson Energy Degraders--copper absorbers which degrade the meson kinetic energy to ~21 Mev, the mean detection energy of the crystal telescope.

Fast Coincidence--coincidence of events in crystals No. 1 and No. 2, such as the passage of a π-meson.

Gate--voltage pulse lasting approximately 10^{-7} sec. which is produced by the gate generator when triggered by the fast coincidence. The gate is 10^{-7} sec. long irrespective of whether the circuit is on "short" or "long" delay.

$\pi - \mu$ Coincidence--coincidence of the gate and an event in the stopping crystal such as would be caused by the passage of a π in crystals No. 1 and No. 2 and its decay in crystal No. 3.

Short Delay--gate starts 2.2×10^{-8} sec. after fast coincidence.

Long Delay--gate starts 19×10^{-8} sec. after fast coincidence.

Short-Delay Count--$\pi - \mu$ coincidence on short delay. This may be either a true π-meson count or an accidental event.

Long-Delay Count--$\pi - \mu$ coincidence on long delay. This can be only an accidental event.

Meson Count--short-delay count minus long-delay count.

$\pi - \mu$ No. 1 Chassis--consists of gate generator, $\pi - \mu$ coincidence and associated distributed amplifiers for channel 1, $\pi - \mu$ No. 2 chassis is a similar chassis for channel 2.

Fast-Coincidence Chassis--consists of two distributed amplifiers A and B and the fast coincidence.

HV No. 1, No. 2, and No. 3--high voltage on the phototubes viewing crystals 1, 2 and 3 respectively.

G_1--the first control grid of the $\pi - \mu$ coincidence. G_1 controls the level of the μ signal required to make a $\pi - \mu$ coincidence.

π Amplifier Bias--determines the level of the fast-coincidence output required to fire the gate generator.

Units, Constants

All energies are in Mev

T_π $\equiv$ Meson kinetic energy in Mev.

A   = Nuclear mass, also "A" used as symbol for nucleus in general.

Z   = Nuclear charge.

R   = Nuclear radius = $1.4A^{1/3} 10^{-13}$ cm.

λ_m = Meson mean free path for absorption in nuclear matter.

λ_p = Proton mean free path in nuclear matter for all processes competing with meson production.

F   = Combined attenuation factor for protons and mesons, also

  = Number of mesons produced/divided by the number of mesons that would have been produced if there had been no attenuation of protons and mesons in the nucleus.

θ = Angle between incident proton and emerging meson in the lab system.

Range = g/cm^2 of material required to stop a charged particle.

$\hbar$ = de Broglie wave length/2π.

APPENDIX

I. Multiple Coulomb Scattering Loss of Mesons

A correction must be made for mesons scattered out of the crystal telescope by multiple Coulomb scattering in the copper meson-energy degraders. This correction has been calculated on the basis of the distribution formulas derived by Eyges[28]. Eyges has extended the theory of Rossi and Greissen[42] to include the effect of energy loss of the scattered particle as it passes through the degrader. He derives the distribution function:*

$$F(t, y, \theta) = \frac{1}{4\pi \sqrt{A_o A_2 - A_1^2}} \exp\left[\frac{-A_o y^2 + 2A_1 y\theta - A_2\theta^2}{4(A_o A_2 - A_1^2)}\right]$$

where:

$$A_n(t) = \int_0^t \frac{(t-\eta)^n}{w^2(\eta)} d\eta \quad n = 0, 1, 2$$

$$w \equiv 2 v P/E_s$$

$v \equiv$ velocity of particle

$P \equiv$ momentum of particle

$E_s \equiv 21.2$ Mev

t   = distance travelled in the absorber

θ = that angle which is the projection on any plane containing the original direction of travel, of the angle between the direction of the incident particle and its final direction of travel.

y   = distance projected on the same plane as for θ and measured perpendicular to the original line of flight.

(Note: distances are measured in radiation lengths for the degrader used.)

* Note some of the numerical factors were misprinted in ref. 28.

The constants A_o, A_1 and A_2 were determined by numerical integration of the range-energy curves for mesons in copper. The range-energy curves were derived from the usual formula:

$$R_m = \frac{M_m}{M_p} \, R_p(E_p)$$

where: $R(E)$ = range of particle with energy E

$$E_p = \frac{M_p}{M_\pi} \, E_m$$

M = mass

$M_m c^2 = 276$ Mev

E = kinetic energy

subscripts: m = meson; p = proton

The range-energy curves for protons in copper were taken from ref 29.

The distribution function gives the probability that the particle will have the coordinates θ and y after traversing a thickness t of degrader

$$\text{Prob}(t, \theta, y) \, d\theta dy = F(t, \theta, y) \, d\theta dy.$$

The above distribution function can be generalized to the experimental situation in which the distribution at a distance L from the back of the degrader is required.

Degrader

Meson Path

Meson Path
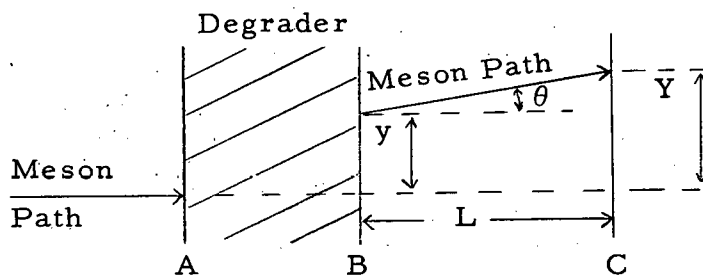
The desired distribution is obtained by making the substitution

$$F_C(t, Y, \theta) = F_B(t, y, \theta) \qquad \begin{array}{l} Y = y - L\theta \\ y = Y + L\theta \end{array}$$

The validity of the above depends upon the fact that there is no change in the angular part of the distribution over the region B to C.

The plane C is taken as the midplane of the stopping crystal. The planes A and B defined the position of the copper degrader. Scattering in the first two crystals is negligible and has been ignored.

If the meson beam, meson-energy degraders, and first two crystals were infinite in the plane perpendicular to the original meson path, the geometry would be "bad" and there would be no correction required. There would be as many mesons scattered into the stopping crystal as scattered out. The dimensions of the system make for neither good nor bad, but for what might be called "mediocre" geometry.

The dimensions of the crystals and the meson beam apertures are:

Beam Aperture		Crystal Dimensions			
			No. 1	No. 2	No. 3
Height	2.9 in.	Height	1.950 in.	2.014 in.	1.844 in.
Width	2.6 in.	Width	1.983 in.	2.013 in.	1.857 in.
		Thickness	0.306 in.	0.202 in.	0.344 in.

In plan view the relative positions of the crystals and meson-energy degraders are shown in Fig. 2. For the moment assume that the apertures, meson-energy degraders, crystals, etc. are of infinite extent in the dimension perpendicular to the plane of Fig. 2, so that multiple-scattering losses need to be calculated in only one plane. The distribution function $F(t, \theta, Y)$ can be applied directly to this situation. The stopping crystal is divided into a number of zones which become progressively smaller near the edges of the crystal where the correction is largest. The aperture is also divided into a number of zones. The contribution of each zone of the aperture to each zone of the stopping crystal is calculated with the provision that no meson is allowed to be in the excluded angle α. A meson whose trajectory lies in the excluded angle α can not fire the gate because it misses crystal No. 1. The angle α of course depends upon the zone in the 3rd crystal under consideration.

For each zone in the stopping crystal the fraction of mesons, H, arriving in the zone is calculated; 1 - H is the fraction lost to each zone. In the limit H may be thought of as a distribution function where $H(Z)$ is the fraction of mesons arriving in the strip dZ, Z units from the center of the crystal.

Now consider the actual case where the geometry is finite in the other dimension. Call this dimention X. The mesons actually arriving in the stopping crystal can then be written as

$$\int_S F(Z)\, F(X)\, dX\, dY \qquad \int_S = \text{integrate over crystal}$$

The justification for this step can be seen as follows. The form of F(t, θ, Z) after integration over θ is given by

$$F(t, Z) = e^{-aZ^2}$$

Now let us guess what the distribution f(t, Z, X) might be where f(t, Z, X) is the two-dimensional distribution function giving the density of particles falling in dXdZ at the coordinate X, Z. Assume

$$f(t, Z, X)\, dZdX = e^{-a(X^2 + Z^2)}\, dZdX$$

Clearly

$$\int f(t, X, Z)\, dX = F(t, Z)$$

$$\int e^{-a(X^2 + Z^2)}\, dX \sim e^{-aZ^2} = F(t, Z)$$

The assumed two-dimensional distribution formula, integrated over X, gives the correct one-dimensional distribution formula in Z.

By means of the distribution function

$$F(Z)\, F(X)\, dZdX$$

the number of mesons scattered out of the stopping crystal is calculated.

II. Attenuation of Protons and Mesons in the Nucleus

R = nuclear radius
= 1.4 $A^{1/3}$ 10^{-13} cm
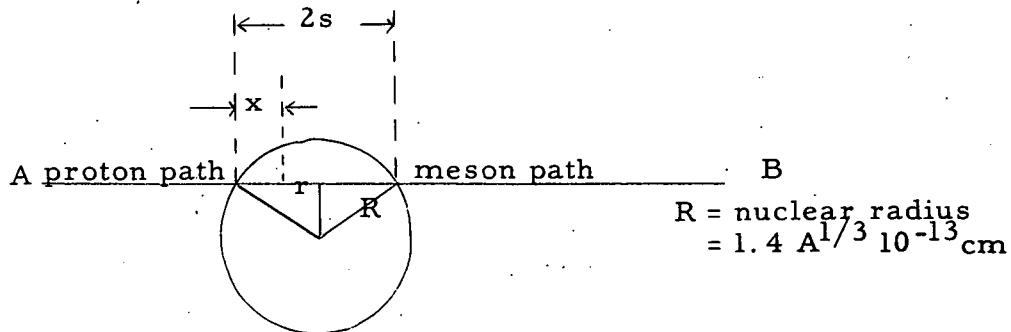
Consider a proton passing through the nucleus along the line AB, and assume that the proton produces a meson at a distance x from the

surface of the nucleus.   The meson continues along the line AB.
Define

I_o $\equiv$ Intensity of incident protons

B $\equiv$ Number of mesons produced/cm^3 in nuclear matter
by unit intensity of protons

λ_p $\equiv$ Proton mean free path in nucleus

λ_m $\equiv$ Meson mean free path in nucleus

$I_o \exp(-x/\lambda_p)\ B \exp(-2s + x)/\lambda_m$ = number of mesons/cm^2
getting out of nucleus which
were formed at x.

Now integrate from 0 to 2s to get contribution throughout nucleus along
line AB.

$$I_o\ B \int_0^{2s} \exp\left[- 2s/\lambda_m - x(1/\lambda_p - 1/\lambda_m)\right]\ dx$$

$$I_o\ B\lambda_1 \left[\exp(-2s/\lambda_m) - \exp(-2s/\lambda_p)\right] \qquad 1/\lambda_1 \equiv 1/\lambda_p - 1/\lambda_m$$

Now integrate over the entire nucleus.   The differential unit of volume
is the annular cylinder of radius r and height 2s

$$\int_0^R I_o\ B\ \lambda_1 \left[\exp(-2s/\lambda_m) - \exp(-2s/\lambda_p)\right] 2\pi r\ dr$$

$$R^2 = r^2 + s^2$$

$$I_o\ B\ \pi\ \lambda_1\ R^2\ B(\lambda_m, \lambda_p, R) \qquad\qquad\qquad (1)$$

where
$$B(\lambda_m, \lambda_p, R) \equiv \left[\begin{array}{l} 1/2(\lambda_m/R)^2 - \left[\exp(-2R/\lambda_p)\right]\left[\lambda_m/R + \lambda_m^2/2R^2\right] \\ -1/2(\lambda_p/R)^2 + \left[\exp(-2R/\lambda_m)\right]\left[\lambda_p/R + \lambda_p^2/2R^2\right] \end{array} \right]$$

If there had been no proton or meson attenuation, the production of
mesons would have been

$$4/3\ \pi\ R^3\ I_o B \qquad\qquad\qquad (2)$$

The attenuation factor, F, is therefore factor (1) divided by factor (2)

$$F = 3/4\ \lambda_1/R\ B(\lambda_m, \lambda_p, R)$$

REFERENCES

1. R. F. Mozley, "Production of π^+-Mesons by X-Rays as a Function of Atomic Number", Phys. Rev. 80, 493 (1) (1950).

2. R. M. Littauer and D. Walker, "Charged Photomesons from Various Nuclei," Phys. Rev. 86, 838 (1952).

3a. D. L. Clark, "The Relative Yield of 20-Mev π^+-Mesons from Seven Elements," Phys. Rev. 81, 313 (A) (1951).

3b. D. L. Clark, "The Production of 40-Mev π^+ and π^- Mesons in Seven Elements by 240-Mev Protons," Phys. Rev. 87, 157 (1) (1952).

4. R. E. Marshak, "Meson Physics," McGraw Hill, 1952, p. 118.

5. D. Hamlin, M. Jakobson, J. Merritt, and A. Schulz, "π^+-Meson Production Cross Section as a Function of Atomic Number," Phys. Rev. 84, 857 (1) (1951).

6. M. M. Block, S. Passman, and W. W. Havens, Jr., "Production of Charged π-Mesons in H, D, C, Cu, and Pb by 381-Mev Protons," Phys. Rev. 88, 1239 (1952).

7a. R. Sagane and W. F. Dudziak, "Dependence of Position Pion Production Cross Sections on Atomic Number at Low Energies," University of California Radiation Laboratory, Report No. UCRL-2317, July, 1953.

7b. R. Sagane and W. F. Dudziak, "The Dependence of the 33-Mev π^+ Production Cross Section on Atomic Number," Phys. Rev. 92, 212 (1) (1953).

8. R. S. White, M. J. Jakobson, and A. G. Schulz, "The Production of Charged Photomesons from Deuterium and Hydrogen," Phys. Rev. 88, 836 (1952).

9. M. Jakobson, A. Schulz, and J. Steinberger, "Detection of Positive π-Mesons by π^+ Decay," Phys. Rev. 81, 894 (1) (1951).

10. C. Wiegand, "Measurement of the Positive π-Meson Lifetime," Phys. Rev. 83, 1085 (1951).

11. C. Wiegand, "Distributed Coincidence Circuit," Rev. Sci. Instr. 21 (12), 975 (1950).

12. R. F. Post, "Resolving Time of the Scintillation Counter," University of California Radiation Laboratory, Report No. UCRL-1675, February, 1952.

13a.   A. G. Schulz, Jr., "The Excitation Function for π^+-Mesons Produced in P-P Collisions at 0° to the Beam," University of California Radiation Laboratory, Report No. UCRL-1756, May, 1952.

13b.   A. G. Schulz, D. Hamlin, M. J. Jakobson, and J. Merritt, "The Excitation Function for π^+-Mesons Produced in P-P Collisions," Phys. Rev. 87, 219 (A) (1952).

14.   D. Hamlin, "Excitation Function for Positive Pions at 90° in Proton-Carbon Collisions," University of California Radiation Laboratory, Report No. UXRL-2414, November, 1953.

15.   W. F. Dudziak, Private Communication.

16.   J. Marshall, L. Marshall, and A. V. Nedzel, "Total Cross Sections of 408-Mev Protons for Hydrogen and Light Elements," Phys. Rev. 91, 767 (1) (1953).

17.   V. A. Nedzel, "Total Cross Sections for 400-Mev Neutrons," Phys. Rev. 90, 169 (1) (1953).

18.   O. Chamberlain, E. Segrè, and C. Wiegand, "Experiments on Proton-Proton Scattering from 120 to 345 Mev," Phys. Rev. 83, 923 (1951).

19.   J. Hadley, E. Kelley, C. Leith, E. Segrè, C. Wiegand, and H. York, "Experiments on N-P Scattering with 90 and 40 Mev Neutrons," Phys. Rev. 75, 351 (1949).

20.   A. L. Bloom, "Experiments on Scattering of 190-Mev Deuterons," University of California Radiation Laboratory, Report No. UCRL-1442, August, 1951.

21.   L. J. Cook, E. M. McMillan, J. M. Peterson, and D. C. Sewell, "Total Cross Sections of Nuclei for 90-Mev Neutrons," Phys. Rev. 75, 7 (1949).

22.   E. Kelley, C. Leith, E. Segrè, and C. Wiegand, "Experiments on N-P Scattering with 260-Mev Neutrons," Phys. Rev. 79, 96 (1950).

23.   P. J. Isaacs, A. M. Scahs, and J. Steinberger, "Total Cross Sections of 60-Mev Mesons in Hydrogen and Deuterium," Phys. Rev. 85, 803 (1952).

24.   G. Yodh, H. L. Anderson, D. E. Nagle, and H. Stadler, "Difference of Hydrogen and Deuterium Total Cross Sections for Charged Pi-Mesons," Phys. Rev. 86, 603 (A) (1952).

25.   H. L. Anderson, E. Fermi, R. Martin, and D. E. Nagle, "Angular Distribution of Pions Scattered by Hydrogen," Phys. Rev. 91, 155 (1953).

26. A. J. Kirschbaum, "Nuclear Absorption Cross Sections for High-Energy Protons," University of California Radiation Laboratory, Report No. UCRL-1967, October, 1952.

27. D. H. Stork, "Total Positive Pion Cross Sections in Complex Nuclei," University of California Radiation Laboratory, Report No. UCRL-2288, July, 1953.

28. L. L. Eyges, "Multiple Scattering with Energy Ions," Phys. Rev. 74, 1535 (1) (1948).

29. W. A. Aron, B. G. Hoffman, and F. C. Williams, "Range-Energy Curves," University of California Radiation Laboratory, Report No. UCRL-121, Second Revision, 1949.

30. R. W. Hales, "Atomic Number Dependence of Neutral Meson Yield from Proton Bombardment," University of California Radiation Laboratory, Report No. UCRL-1836, June, 1952.

31. H. L. Anderson, E. Fermi, E. A. Long, and D. F. Nagle, "Total Cross Sections of Positive Pions in Hydrogen," Phys. Rev. 85, 936 (1) (1952).

32. E. C. Fowler, W. B. Fowler, R. P. Shutt, A. M. Thorndike, and W. L. Whittemore, "Angular Distribution of 53-Mev Positive Pions Scattered by Protons," Phys. Rev. 86, 1053 (1) (1952).

33. G. Goldhaber, "Study of Elastic Pion-Hydrogen Scattering in Photographic Emulsions," Phys. Rev. 89, 1187 (1953).

34. A. L. Anderson, E. Fermi, D. E. Nagle, and G. B. Yodh, "Angular Distribution of Pions Scattered by Hydrogen," Phys. Rev. 86, 793 (1) (1952).

35. H. L. Anderson, E. Fermi, E. A. Long, R. Martin, and D. E. Nagle, "Total Cross Sections of Negative Pions in Hydrogen," Phys. Rev. 85, 934 (1952).

36. S. L. Leonard, "Yield of Charged Pions at 180° to the Beam by 340-Mev Protons on Carbon," University of California Radiation Laboratory, Report No. UCRL-2210, May, 1953.

37. J. B. Cladis, "Nuclear Momentum Distributions in Deuterium and Carbon Inferred from Proton Scattering," Thesis, University of California Radiation Laboratory, Report No. UCRL-1621, January, 1952.

38. R. Durbin, H. Loar, J. Steinberger, "The Absorption of Pions by Deuterons," Phys. Rev. 84, 581 (1951).

39. S. Passman, M. M. Block, W. W. Havens, Jr., "Excitation Function for Charged π-Meson Production in Hydrogen and Carbon by 345- to 380-Mev Protons," Phys. Rev. 88, 1247 (1952).

40. M. L. Stevenson, "The Angular Distribution of the Reaction $p + p \rightarrow d + \pi^+$ at 338 Mev," University of California Radiation Laboratory, Report No. UCRL-2188, April, 1953.

41. W. F. Cartwright, C. Richman, M. N. Whitehead, and H. A. Wilcox, "The Production of Positive Pions by 341-Mev Protons on Protons," Phys. Rev. **91**, 677 (1953).

42. B. Rossi and K. Greiser, "Cosmic Ray Theory," Rev. Modern Phys. **13**, 240 (1941).

Table I   Series I

$$T_\pi = 53 \text{ Mev}$$

Target	(Relative) $d^2\sigma/dE\, d\Omega$
Be	11.4 ± 2.0
C	15.3 ± 3.7
Al	21.7 ± 4.5
Fe	50.0 ± 10.0
Cu	42.0 ± 7.0
Ag	60.0 ± 10.0
Pb	50.0 ± 12.0

Table II   Series II

$$d^2\sigma/dE\, d\Omega\ \text{cm}^2 \times 10^{-30}\ \text{Mev}^{-1}\ \text{steradian}^{-1}$$

T_π	Be^9	B^{10}	$B^{(Natural)}$	C^{12}
34 Mev	4.2 ± 1.6	3.5 ± 1.4	4.3 ± 1.4	7.1 ± 1.8
51	8.5 ± 2.2	7.6 ± 2.1	8.1 ± 2.3	11.9 ± 2.5
69	7.8 ± 2.9	15.0 ± 2.9	14.6 ± 3.1	15.4 ± 3.6
88	17.9 ± 3.7	13.7 ± 3.2	15.4 ± 3.8	16.0 ± 4.3
110	10.7 ± 4.4	13.0 ± 4.0	10.3 ± 3.6	14.8 ± 4.7
129	5.3 ± 3.8	7.7 ± 4.8	3.6 ± 3.6	11.2 ± 4.6

$$d\sigma/d\Omega\ \text{cm}^2 \times 10^{-28}\ \text{steradian}^{-1}$$

	Be^9	B^{10}	$B^{(Natural)}$	C^{12}
	15.0 ± 2.2	16.7 ± 2.2	21.0 ± 2.3	21.0 ± 2.5

Table III Series III

$$d^2\sigma/dE\,d\Omega\ cm^2 \times 10^{-30}\ Mev^{-1}\ steradian^{-1}$$

T_π	C	Cu	Pb
52	9.7 ± 1.6	21.8 ± 2.9	46.7 ± 7.4
65	15.0 ± 2.2		
88	19.7 ± 1.7	32.4 ± 4.5	73.7 ± 9.8
147	11.4 ± 1.5	23.6 ± 4.7	40.8 ± 9.5

Table IV Deuterium Data of Series IV

All Corrections Prior to Subtraction Have Been Made.
Relative $d^2\sigma/dE\,d\Omega$ are Plotted.

Target. Full, Run No. 4, 1000 psi

T_π	43 Mev	52	70	89	111	130
	10.1 ± 2.7	19.0 ± 3.1	28.4 ± 3.2	24.6 ± 2.5	12.4 ± 2.7	13.1 ± 2.7

Target. Full, Run No. 5, 2000 psi

T_π	47 Mev	56	66	74	82	92	104	114	132
	20.4 ± 2.0		28.4 ± 3.3		22.7 ± 2.3		15.1 ± 2.3		7.4 ± 2.1
		24.9 ± 2.2		27.9 ± 1.7		21.5 ± 2.5		10.6 ± 2.6	

Target. Empty - (Normalized for Subtraction)

T_π	35 Mev	45	65	85	106	125	148
	3.61 ± 0.66		3.82 ± 1.0		1.92 ± 0.69		-0.53 ± 1.8
		2.17 ± 0.66		3.2 ± 1.2		2.5 ± 0.6	

Table V

Deuterium Spectrum

$$d^2\sigma/dE \, d\Omega = cm^2 \times 10^{-30} \, Mev^{-1} \, steradian^{-1}$$

T_π	42	50	60	70	80	90	100	110	120	130	140
$\dfrac{d^2\sigma}{dE d\Omega}$	1.77	2.81	4.0	4.41	4.04	3.36	2.73	2.10	1.50	0.90	0.45
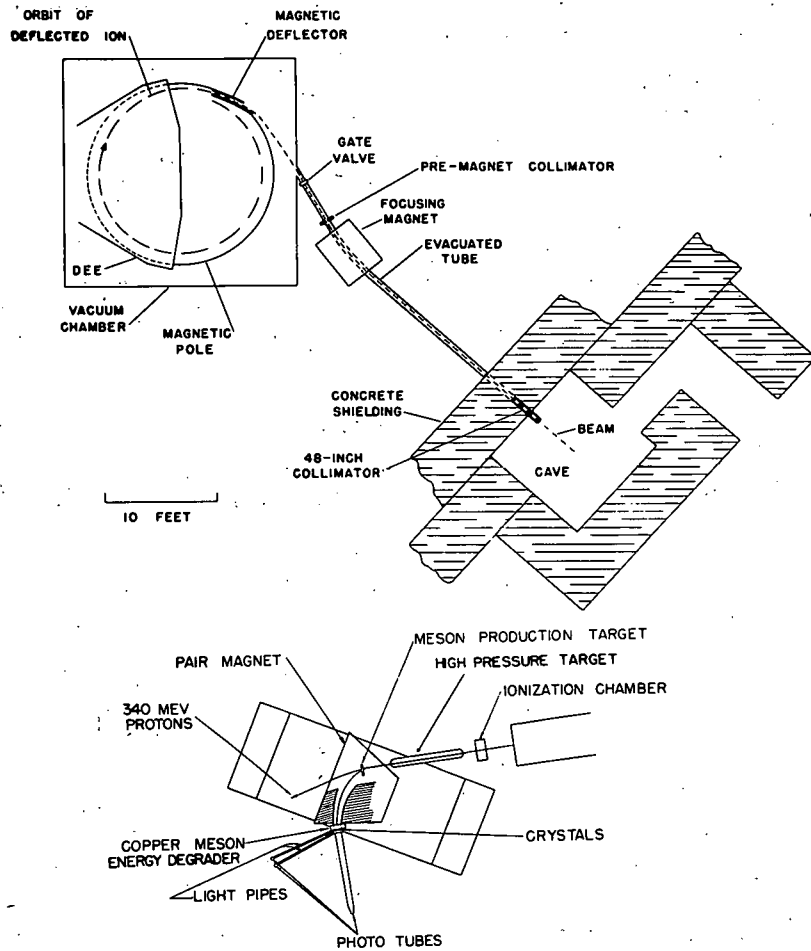
Fig. 1a, b—General layout.
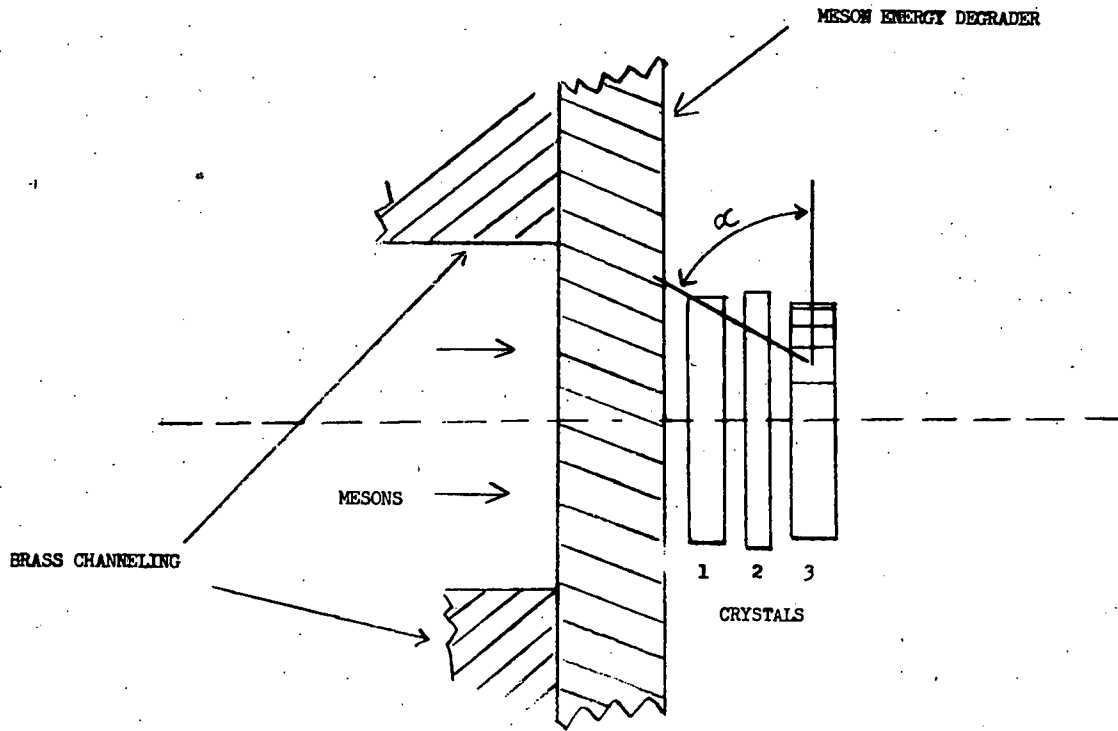
Fig. 2—Layout of crystal telescope and meson energy degrader.
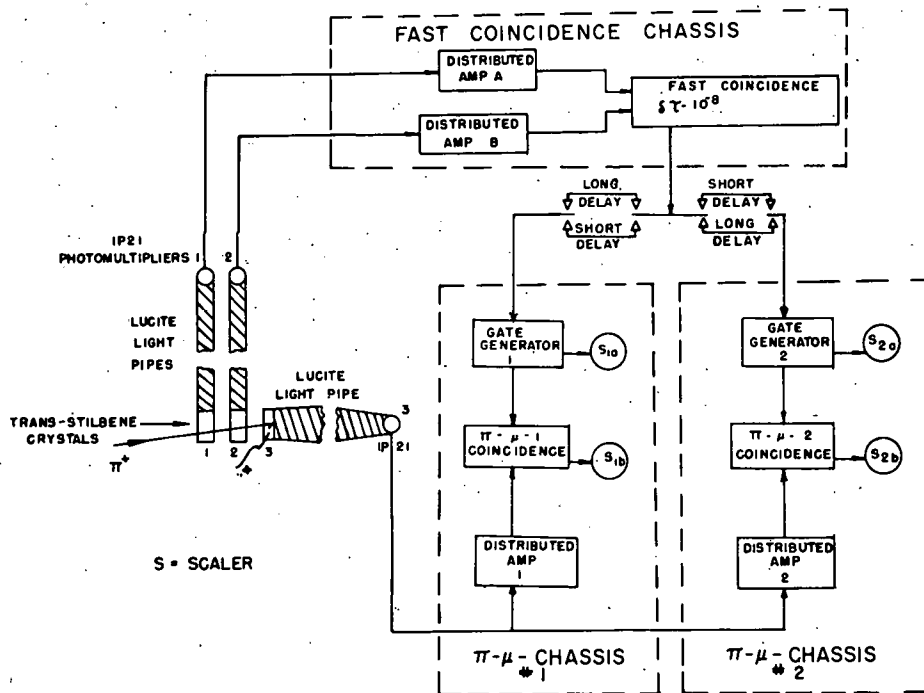
Fig. 3—Block diagram electronics.
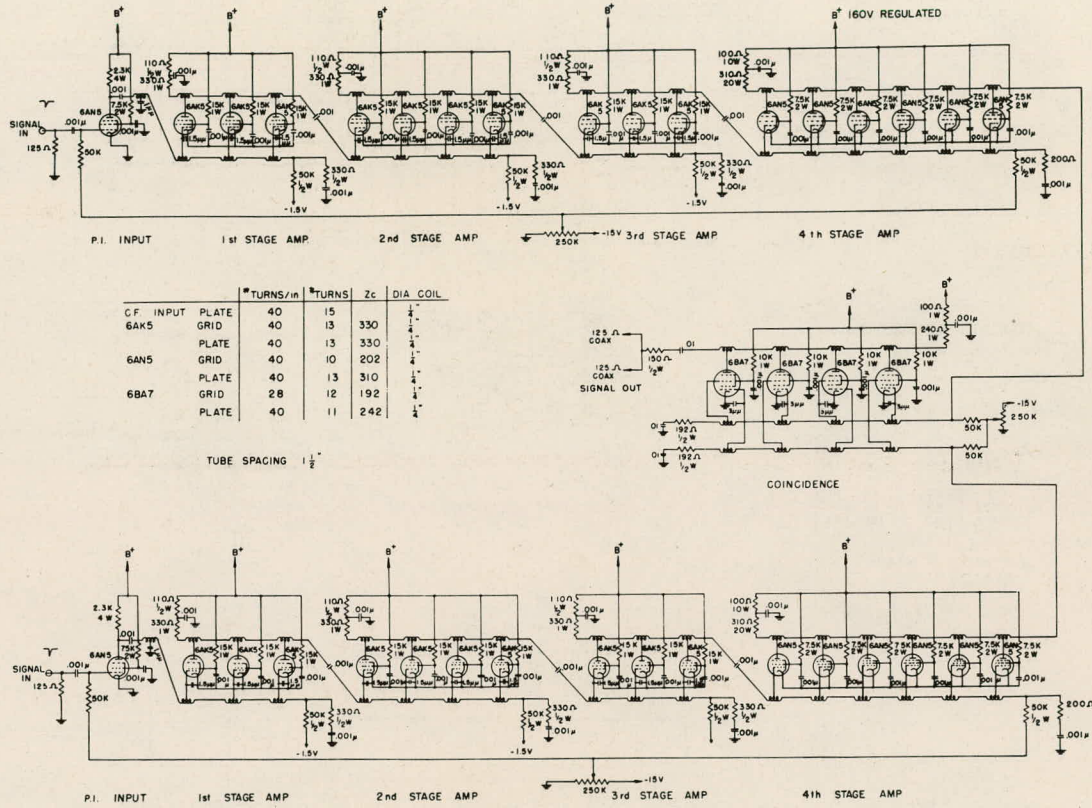
Fig. 4—Circuit diagram for fast coincidence chassis.
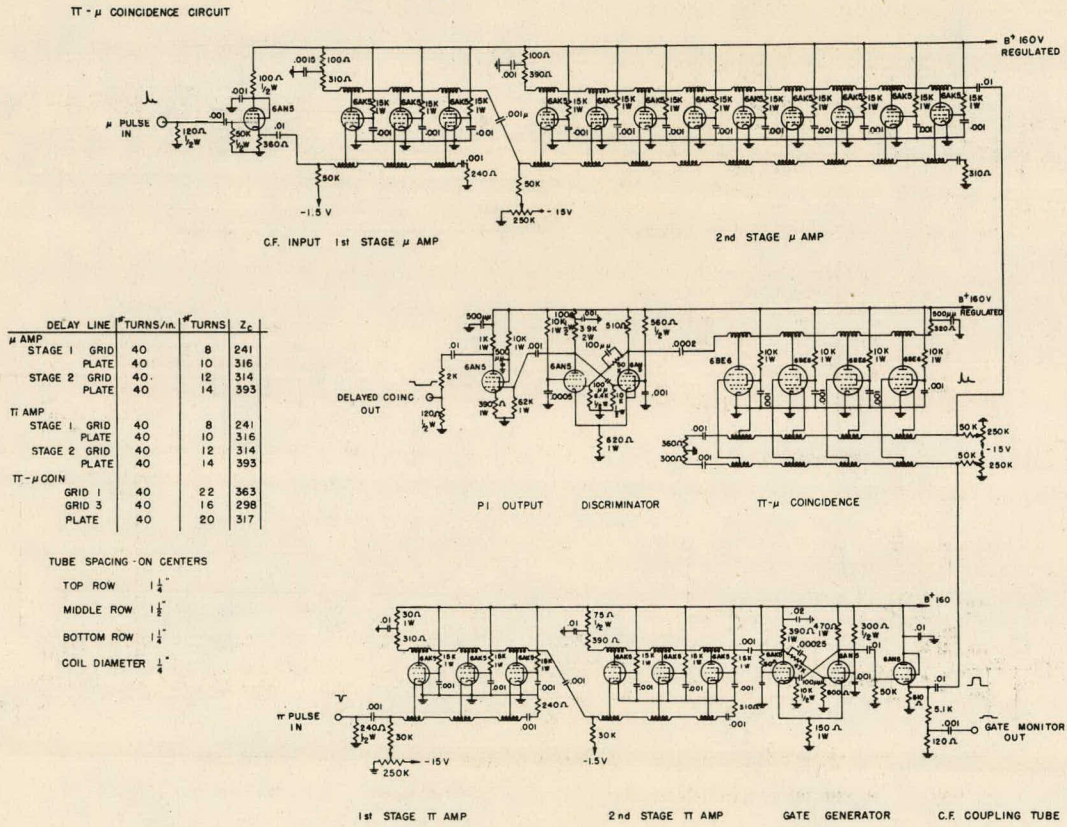
Fig. 5—Circuit diagram for π - μ chassis.
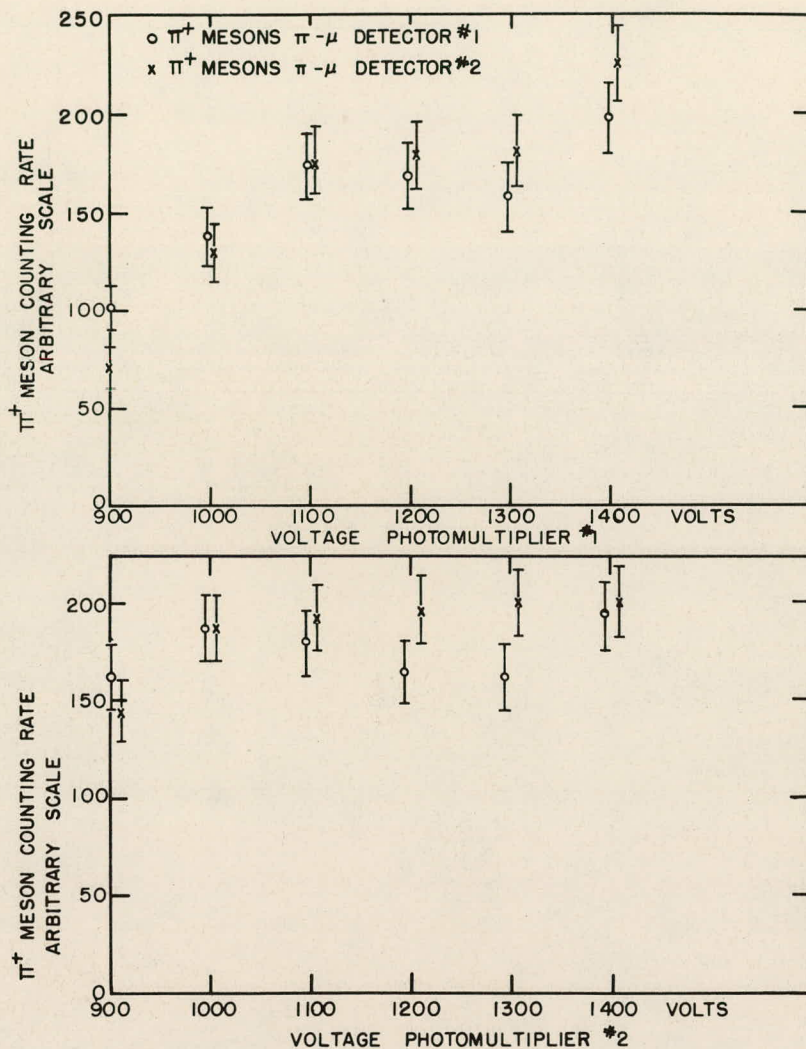
Fig. 6 — High voltage plateaus for phototubes
No. 1 and No. 2.
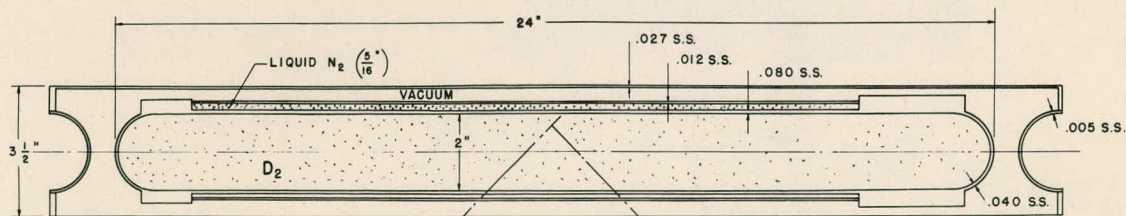
Fig. 7 — Schematic of high pressure deuterium target.
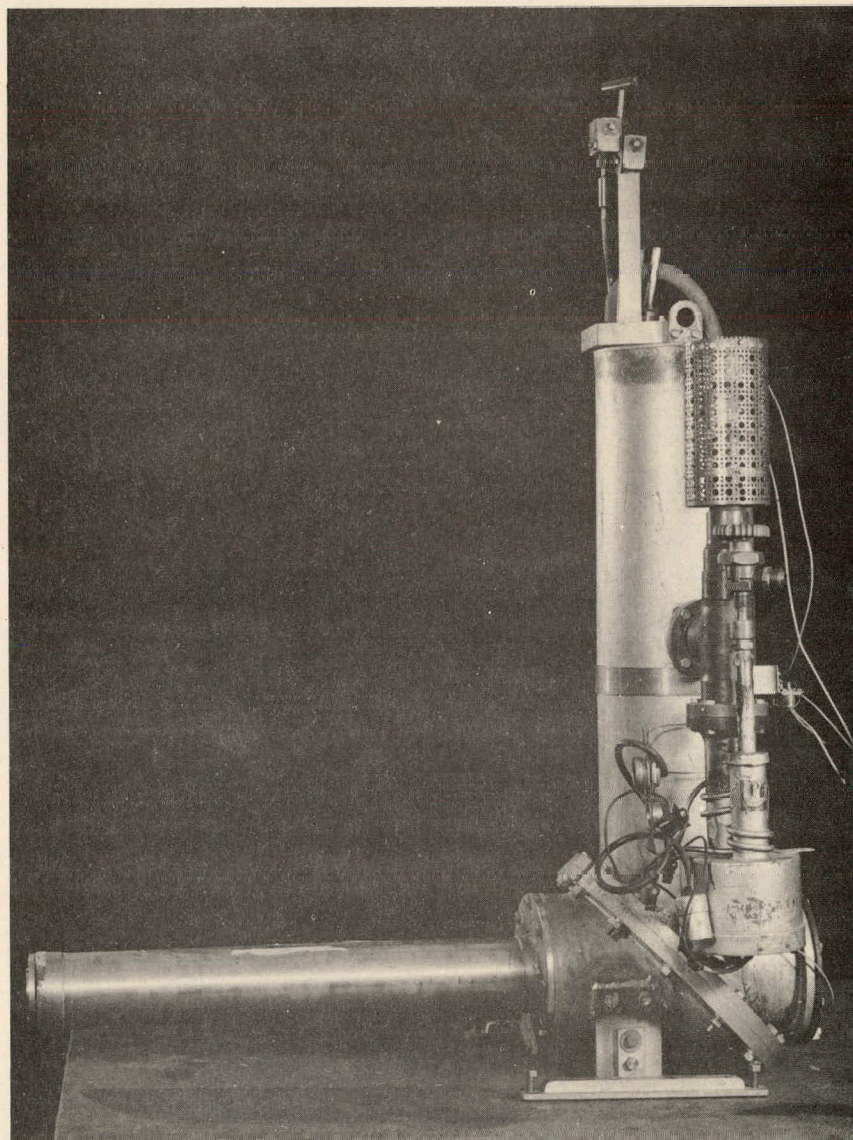
Fig. 8 — High pressure deuterium target.
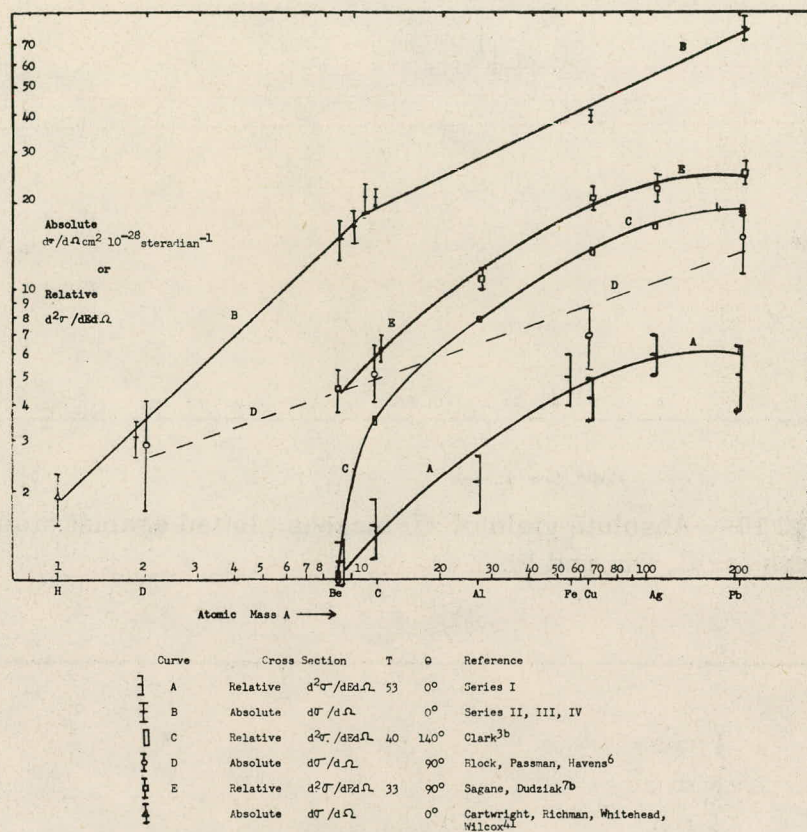
Fig. 9 — Comparison of π^+ yield by different experiments.
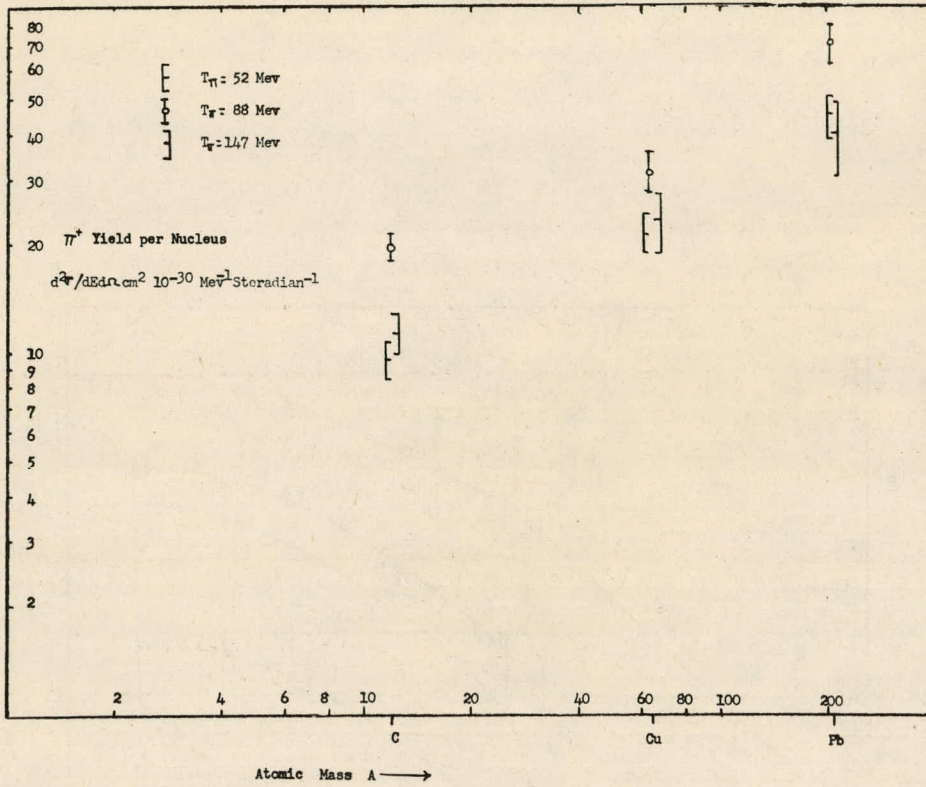
Fig. 10 — Absolute yield of π^+-mesons plotted against atomic mass for C, Cu, and Pb.
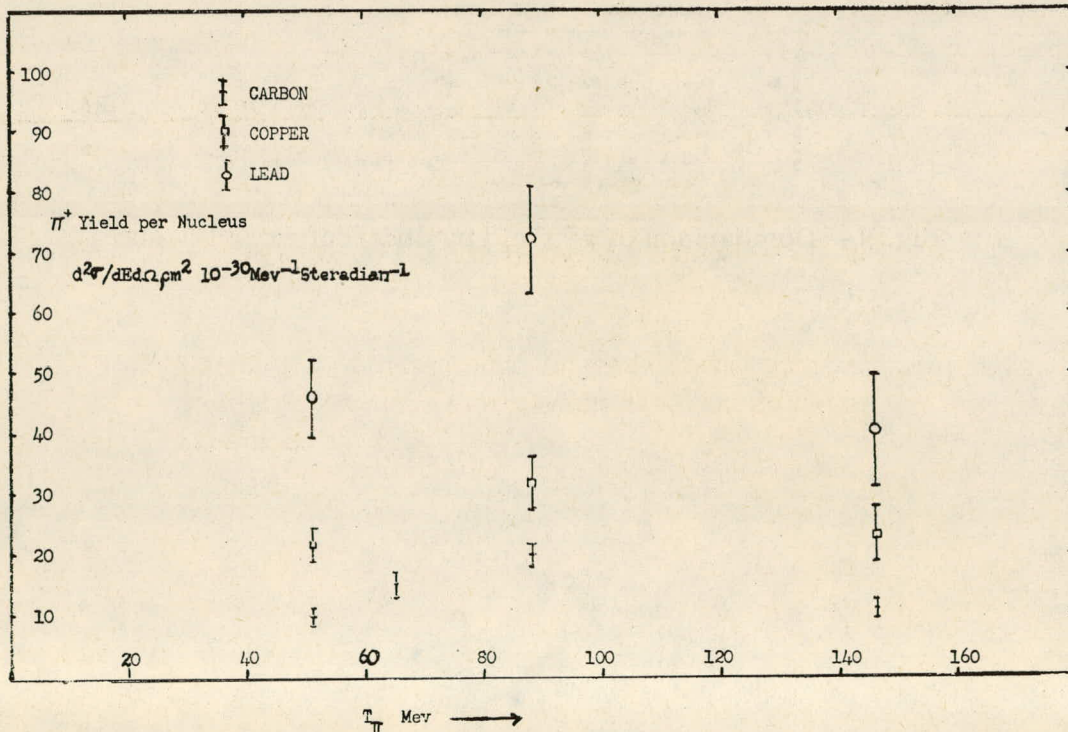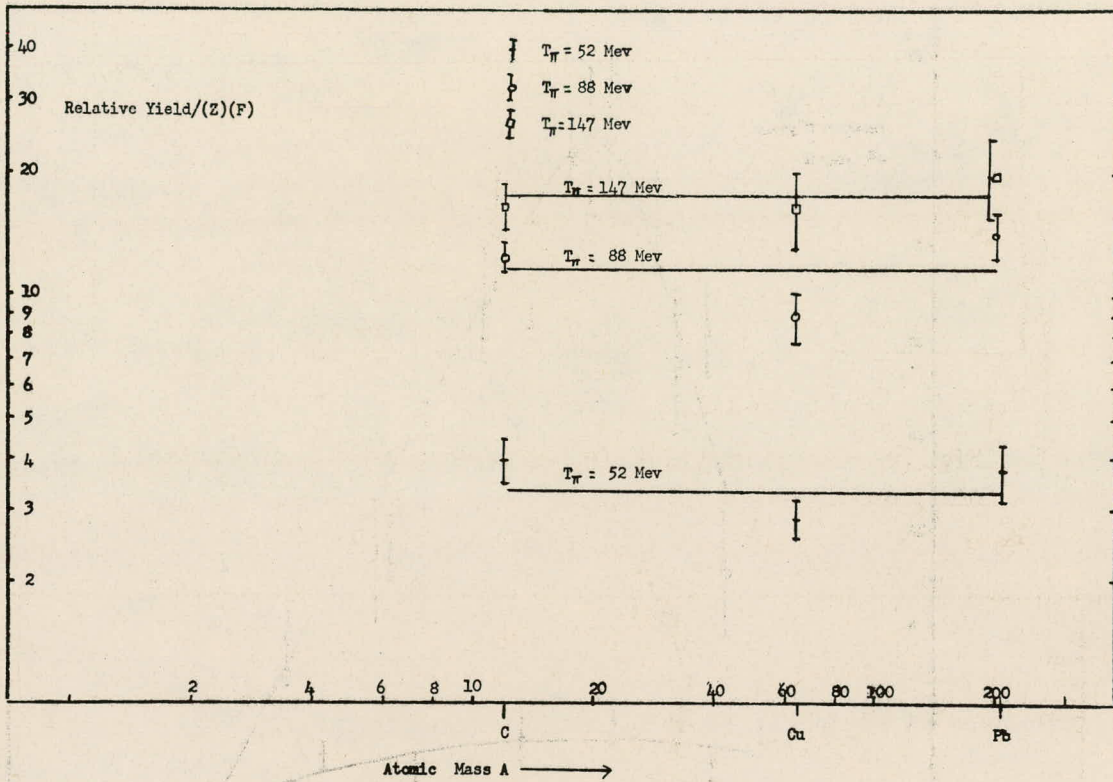

Fig. 11 — Spectra for π^+ yield from C, Cu, and Pb.

Fig. 12 — Relative π^+ yield divided by (Z) (F).

Series IV Run 5, Target Full 1000 psi

Series IV Run 6, Target Full 2000 psi

Series IV   Target Empty (normalized for subtraction)

Relative π^+ yield

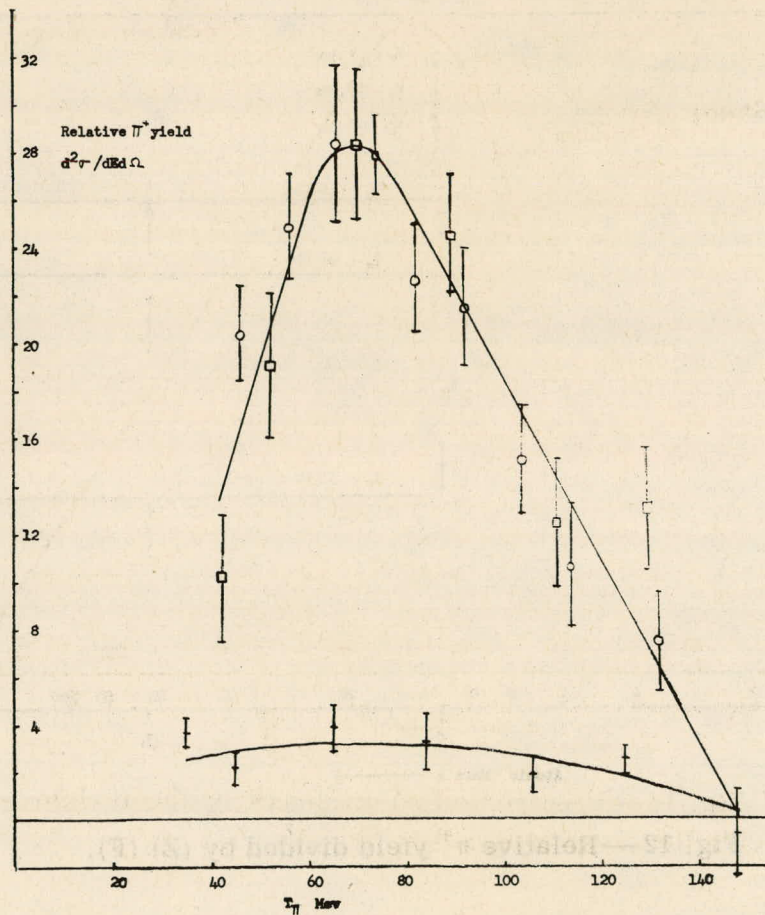$d^2\sigma\,/d\mathrm{E}d\,\Omega$

T_π Mev

Fig. 13 — Spectrum of π^+-mesons from deuterium plus high pressure target. (Note all corrections have been made.)
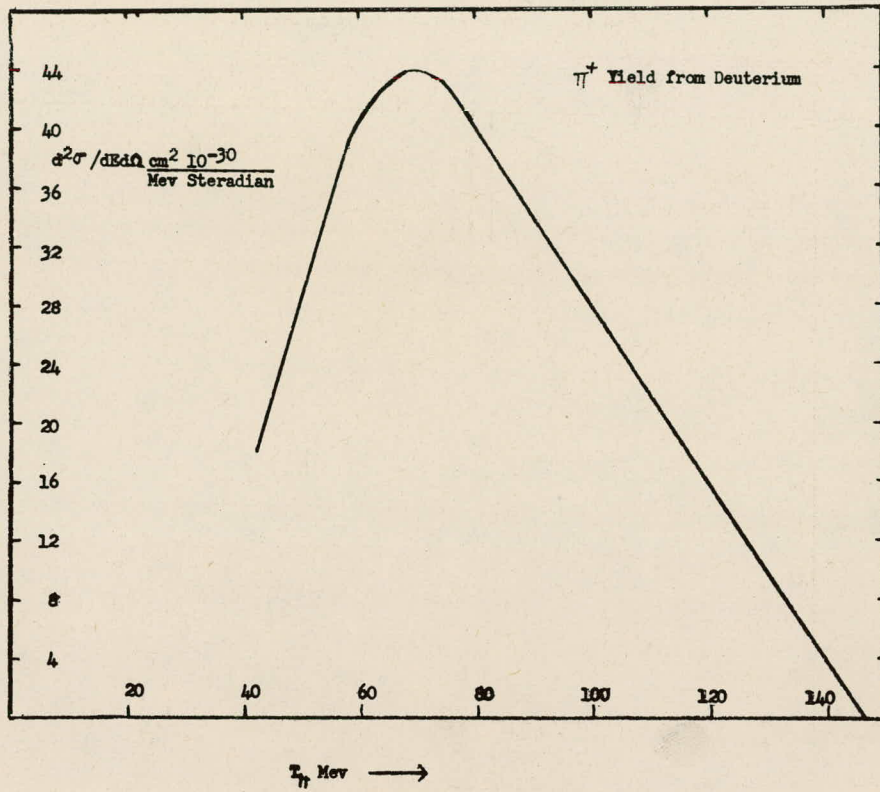
Fig. 14 —Spectrum of π^+-mesons from deuterium
for the reaction $P + D \rightarrow \pi^+ + A'$.